FLUSH PROBE STUDIES OF
PLASMA FLOW OVER A FLAT PLATE

by

CLINTON RANDY GILES

B.Sc., University of Victoria, Victoria, 1976

A THESIS SUBMITTED IN PARTIAL FULFILLMENT

OF THE REQUIREMENTS FOR THE DEGREE OF

MASTER OF SCIENCE

in the Department

of

Physics

We accept this thesis as conforming

to the required standard

[redacted]

ABSTRACT

Supervisor: Dr. Reginald M. Clements

A method of utilizing a planar geometry probe to measure flow properties of a plasma has been developed. No previous work exists in the literature on using a Langmuir probe to examine the viscous boundary layer around the probe. The technique involves applying a step voltage to a flat plate probe in a flowing continuum plasma and observing the relaxation of the ion current to flush probes mounted in the plate. The time it takes to relax to a new equilibrium ion current equals the flow time along the ion sheath edge from the flat plate's leading edge to the flush probe.

A simplified theory was developed to predict the relaxation phenomenon for the flat plate ion current when the ion sheath edge was outside the viscous boundary layer. The purpose of this theory was primarily to explain the ion current signal which was used in the relaxation measurements. The success of the model was evidenced by agreement (within 25%) between theory and experiment when measuring the amplitude of the ion current spike that resulted from the voltage step.

A rigourous theory proposed in this thesis, gave numerical results for the ion sheath thickness as a function of plate voltage when the ion sheath edge is inside the hydrodynamic boundary layer. This theory was based on Stahl and Su's technique of matching the quasineutral solution to the ion sheath solution of the equations

governing the plasma behaviour around the flat plate. There is no earlier model for the ion sheath completely inside the viscous boundary layer when ion convection is an important transport mechanism. This new model allowed the step voltage method to be used in measuring flow times in the viscous boundary layer which were then compared to an approximate fluid model calculated using Von Karman's momentum integral. Agreement to within 10% between the flush probe relaxation times and the fluid approximation was observed. It is felt that this new method of plasma flow measurements is amenable to further development as a general diagnostic technique in flowing plasma studies.

Signed 

TABLE OF CONTENTS

LIST OF TABLES

LIST OF FIGURES

LIST OF SYMBOLS

All quantities are in SI units unless stated otherwise. Subscript α denotes either + or - which correspond to ion and electron properties respectively. Subscript "o" denotes a property of the undisturbed plasma.

A	An Average Boundary Layer Temperature	
A_1	The region of the Pulsed Probe Signal where the Signal has relaxed	
a	$\delta(X) = aX^{\frac{1}{2}}$	(a constant for determining the viscous boundary layer thickness)
a_1	$= 9\mu_{+o}\varepsilon_o V_F^2/8N_o e$	(a constant in the equations for the ion current to a flat plate)
B_1, B_2	Regions of the Pulsed Probe Signal where the Signal is still relaxing	
b	Flush Probe Diameter	
C, C_1, C_2	Constants of Integration	
$\tilde{D}_\alpha$	Charged Particle Diffusion Coefficient	
$\tilde{D}_a$	Ambipolar Diffusion Coefficient	
D_α	Nondimensionalized Diffusion Coefficient	
E	Electric Field	
e	Electronic Charge	
f_1	$Y_s = l^{\frac{1}{2}} f_1$	f_1, f_2, and f_3 describe the electrical properties of the flat plate using the theory of section 2.5.
f_2	$I_{dim} = (N_o/l^{\frac{1}{2}})\, f_2$	
f_3	$V = (lN_o)^{\frac{1}{2}} f_3$	
$g(\ )$	$C_2 = g(C_1)$	(an arbitrary function)
$H(\ )$	Unit Step Function	

h	An arbitrary Distance away from the Flat Plate Probe
h_1	$= j_{\tilde{t}=0+} - j_{\tilde{t}=0-}$
h_2	$= j_{\tilde{t}=\infty} - j_{\tilde{t}=0-}$
I	Ion Current to a Cylindrical Probe (μA)
I_α	Nondimensionalized Charge Particle Current Density
I_{dim}	Current Density to the Flat Plate
I_s	Ion Current to a Spherical Probe
I_1, I_2	Integrals used in evaluating $\delta(X)$
j_α	Charged Particle Current Density
$j_{\tilde{t}=k}$	Ion Current Density at $\tilde{t} = k$
$j_{t,sat}$	Ion Saturation Current Density
j_T	Convection Ion Current Density
j_D	Diffusion Ion Current Density
K	Plasma Equilibrium Parameter
k	Boltzmann Constant
l	A Typical Reference Length
l_p	Cylindrical Probe Length (cm)
M	An Alkali Atom
m_-	Electron Rest Mass
N_α	Charged Particle Density
N_o	Freestream Charged Particle Density ($N_{\alpha o} = N_o$
n_α	Nondimensionalized Charged Particle Density
P	Prandtl Number
P_α	Charged Particle Production Rate
p	Gas Pressure (Torr)
R	Spherical Probe Radius

R_e	Electric Reynolds Number
r_s	Ion Sheath Radius around a Cylindrical or Spherical Probe
S	$= 2I_+ \tilde{D}_{+o} l/U_o \lambda_D^2$ (a constant from the ion sheath equation in section 2.5.3)
T	Nondimensionalized Flame Temperature
$\tilde{T}$	Flame Temperature
$\tilde{T}_o$	Freestream Plasma Temperature ($\tilde{T}_o = \tilde{T}_{\alpha o}$)
$\tilde{T}_w$	Probe Temperature
$\tilde{T}_\alpha$	Charged Particle Temperature
t	Nondimensionalized time ($U_o \tilde{t}/l$)
$\tilde{t}$	Time
U	Plasma Speed
$U_{average}$	Average Speed between the Flat Plate's Leading Edge and the Point of Interest
$U_{measured}$	Experimental Value of $U_{average}$
U_{theory}	Theoretical value of $U_{average}$
u	Nondimensionalized Plasma Speed ($= U/U_o$)
V	Probe Voltage
V_F	Floating Potential
V_f	Probe Voltage after a Voltage Change
V_i	Probe Voltage before a Voltage Change
V_p	A Typical Probe Voltage
V_{plasma}	Plasma Potential
v	Plasma Speed Perpendicular to the Flat Plate
X	Distance Downstream from the Flat Plate's Leading Edge
$\hat{x}$	A Unit Vector Parallel to the Flat Plate's Surface
Y	Perpendicular Distance away from the Flat Plate

Y_{fo}	Distance the Electron Edge Recedes from the Flat Plate at $\tilde{t}=0^+$ when the Probe Voltage Changes
Y_s	Sheath Edge Position
y	Nondimensionalized Distance Away from the Flat Plate
$\hat{y}$	A unit Vector Normal to the Flat Plate's Surface
y_s	Nondimensionalized Sheath Edge Position
α	$= \lambda_D/l$ (Ratio of Debye Length to a Probe Reference Length)
α_r	Ion-Electron Recombination Coefficient
β	$= (D_{ao}/U_o a^2)^{\frac{1}{2}}$ (A constant from the Quasineutral Equation in section 2.5.2)
$\underline{\Gamma}_\alpha$	Charged Particle Flux
γ	$y/x^{\frac{1}{2}}$
Δ	A Small Number $0 < \Delta << 1$
$\delta(X)$	Viscous and Thermal Boundary Layer Thickness
$\delta_{thermal}$	Thermal Boundary Layer Thickness
$\delta_v(X)$	Viscous Boundary Layer Thickness
ε_o	Permittivity of Free Space
ζ	$= Y R_e^{\frac{1}{2}}$, a Dummy Variable in Integration
η	$= Y/\delta_v(X)$ (Ratio of the Distance from the Flat Plate to the Viscous Boundary Layer Thickness)
θ	Azimuthal Angle From the Stagnation Point of a Spherical Probe in a Flowing Plasma
λ	Mean Free Path
λ_D	Debye Length
μ	Kinematic Viscosity
μ_w	Kinematic Viscosity at the Probe Surface
μ_o	Kinematic Viscosity in the Freestream Plasma
μ_α	Charge Particle Mobility Coefficient

ν	$= \tilde{T}_w/\tilde{T}_o$
ρ	Mass Density of Flame Gas
ρ_o	Mass Density of Flame Gas at Freestream Plasma Temperature
ρ_w	Mass Density of Flame Gas at Probe Temperature
σ', σ	Ion Current Spike Parameters
τ	Ion Current Relaxation Time
τ_1, τ_2	Time Intervals for Determining the Relaxation Time from the PHA Signal
Φ_i	Ionization Potential of Alkali Metal Atoms
ϕ	Nondimensionalized Probe Potential
χ	Ratio of Probe Voltage to Electron Energy $(= eV/k\tilde{T}_{-o})$
χ_p	Ratio of a Typical Probe Voltage to Electron Energy
ψ	Probe Potential Nondimensionalized w.r.t. a typical Probe Voltage, V_p

ACKNOWLEDGEMENTS

I would like to thank my supervisor, Dr. R.M. Clements, for his thoughtful supervision and encouragement through the course of my work. I am also thankful for the many hours he freely gave in constructive discussion of my project. I am indebted to Dr. P.R. Smy* for making clear the mechanisms involved in the probe step voltage response and also for his supportive enthusiasm throughout my studies. Mr. D. Way-Nee* very kindly constructed the flat plate assembly used in the experiment.

I am indebted to the National Research Council for its financial support in the last two years.

* University of Alberta, Edmonton

CHAPTER 1

INTRODUCTION

The first major advances in the use of probes in plasma diagnostics can be attributed to Langmuir in 1924 during his studies of electrical conduction in low-pressure gas discharges. Probes have since been used to measure ion and electron densities and temperatures in ionized media which include electric discharges (Langmuir, 1924), re-entry vehicle flow fields (Sonin, 1967), ionizing shock waves (Burke, 1968), flames (Clements and Smy, 1969) and MHD flows (reviewed by Self and Kruger, 1977). The method of using the electric probe is to insert one or more metallic electrodes in the plasma and to connect the electrodes to a voltage supply. The probe's current-voltage characteristic may then reveal properties of the plasma. In the single probe configuration, there is one electrode and the return path for the current is some conducting wall in good electrical contact with the plasma (for example, one end of a gas discharge tube or the burner for a flame plasma). The double probe normally consists of two electrodes, usually of equal area and the current characteristics are measured. These two basic probe configurations are illustrated in Fig. 1.1.

Probes can be operated in different plasma regimes where certain parameters characterize the system and may lead to simplification of the theory. When $\lambda << \ell$ where ℓ is a probe reference length and λ is the smallest mean free path of particles in the plasma, the probe is in the continuum regime. In this case, a plasma particle

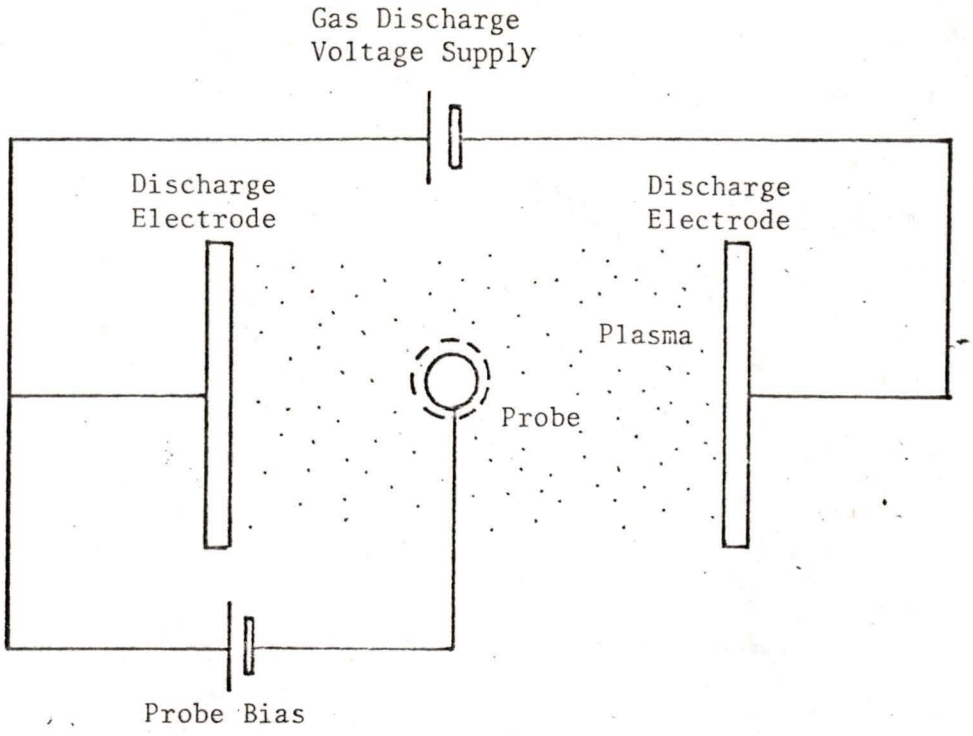

i. Single Probe Configuration

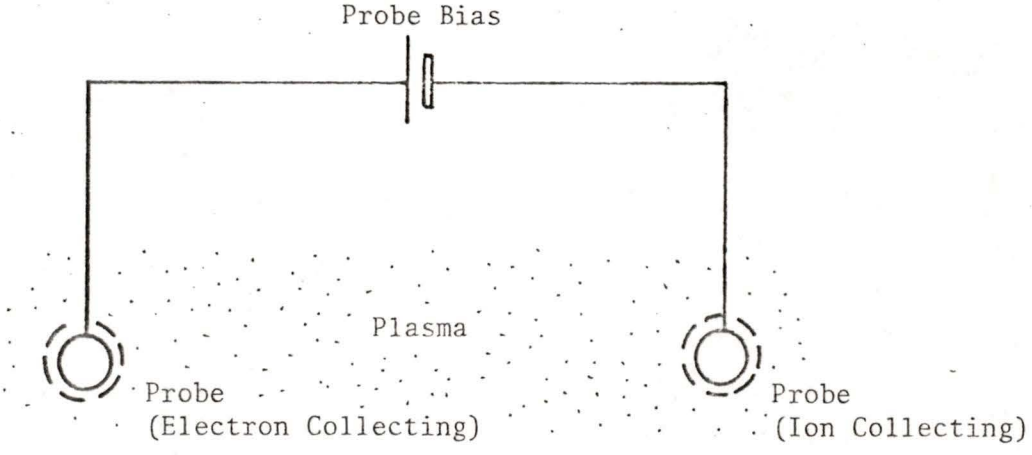

ii. Double Probe Configuration

Figure 1.1. Single and Double Probe Configurations

(Dotted lines around the probes indicate regions of disturbed plasma)

suffers many collisions when moving one characteristic length. Otherwise, the probe is said to be operating in the collisionless regime. Throughout this thesis only collisional plasmas will be examined. Another parameter which is particularly important is the dimensionless quantity $R_e = U_o l/\tilde{D}_{+o}$. U_o is the plasma flow speed far from the probe and $\tilde{D}_{+o}$ is the ion diffusion coefficient where subscript "o" indicates the value in the undisturbed plasma. R_e is the Electric Reynolds number and indicates the relative importance of ion convection to ion diffusion in the plasma; $R_e \to 0$ as diffusion dominates while $R_e \to \infty$ as convection becomes the important ion transport mechanism. When $R_e > 1$ the plasma is said to be flowing. The probe studies in this thesis will be for a probe in a weakly ionized flowing plasma operating in a continuum regime.

Nondimensionalizing Poisson's equation reveals one other important parameter. With the Debye length $\lambda_D = (\varepsilon_o k T_{-o}/N_o e^2)^{\frac{1}{2}}$ ($k \equiv$ Boltzmann constant; $\varepsilon_o \equiv$ permittivity of free space; $e \equiv$ electronic charge; $N_o \equiv$ charged particle density; $\tilde{T}_{-o} \equiv$ mean temperature of the electrons) and $\chi_p = eV_p/k\tilde{T}_{-o}$ (V_p a typical probe voltage), the dimensionless Poisson's equation is

$$\chi_p(\lambda_D/l)^2 \nabla^2\psi = -(n_+ - n_-)$$

$\psi = V/V_p$, ∇^2 is the dimensionless Laplacian operator and $\alpha = +$ or $-$. Poisson's equation is singular as $\chi_p(\lambda_D/l)^2 \to 0$ and the ion and electron densities are equal except for a thin layer close to the probe where only ions are present. Since the Debye length is a measure of the range of influence of a charged particle (Krall

and Trivelpiece. 1974), the singularity as $\chi_p(\lambda_D/l)^2$ vanishes can be interpreted as saying that the particle weakly interacts over a probe dimension and so the plasma disturbance is confined to being very close to the probe. In the limit as $\chi_p(\lambda_D/l)^2 \to \infty$, the ion and electron densities are negligible and allows for an ion sheath to extend over the whole region of interest. For $\chi_p(\lambda_D/l)^2 > 1$, the sheath is said to be thick.

The experimental arrangement for making the probe measurements is often very simple but the problem arises that the plasma is disturbed by the probe's presence. Away from the probe, the plasma is quasi-neutral, that is, there are equal numbers of electrons and ions in the plasma though their density may be less than the freestream density. Close to the probe, the ion and electron concentrations may differ greatly. In the quasineutral region, only a weak electric field exists and the voltage drop over the region is characteristically $k\tilde{T}_{-o}/e$. The mechanism of ion and electron motion in the quasineutral region is ambipolar diffusion and possibly bulk plasma motion. In the usual experimental situation for the single probe, the probe is biased negatively with respect to the plasma and the region closest to the probe has a much higher concentration of ions than electrons. Large electric fields can result in this ion sheath and ion mobility dominates as the transport method unless $|V_{plasma}| < |V| < |V_F|$ (V_F is the plasma floating potential) and ion diffusion may be significant (see Fig. 1.2).

In an experiment with a probe, the current of both ions and electrons will contribute to the net current. The measured current as a function

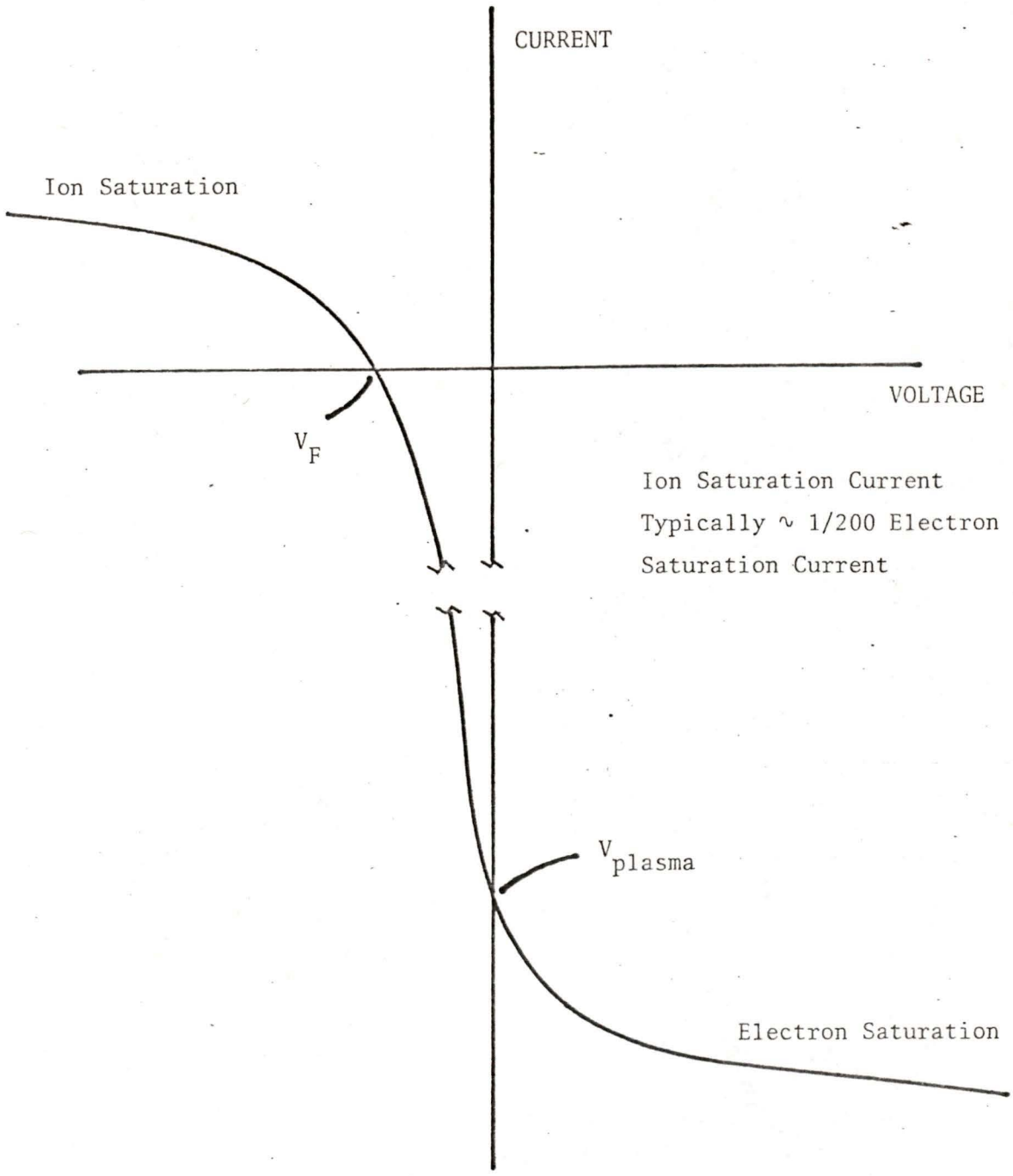

Figure 1.2. A Typical Single Probe Characteristic

of voltage applied to the single probe is similar to that illustrated in Fig. 1.2. Three points are of special interest in Fig. 1.2. First is the floating potential, V_F which an isolated probe will assume when immersed in the plasma. At this potential, the net current to the probe is zero. Secondly, there is the plasma potential, V_{plasma} where an object does not electrically disturb the plasma. Electrons are lighter and more mobile than the ions in a plasma so if the two particles are at equal temperatures, the thermal electron flux through a given surface will be much larger than the thermal ion flux. At plasma potential then, the net current to a conductor is electron current. Finally from Fig. 1.2, if a probe is biased sufficiently negative, the electron current will become negligible compared to the ion current and the ion collection will be limited by the ions' mobility and diffusivity. This region of the probe current-voltage characteristic where the electron current is very small is called the ion saturation region. Electron saturation of a single probe is difficult to attain because the electrons are very mobile and large perturbations of the plasma are likely before electron saturation occurs (i.e., the electrons may be largely depleted by high electron currents to the probe before the ion current is negligible).

After Langmuir and Mott-Smith (1926) studied electric probes in collisionless plasmas, probably the most significant result in probe theory was the continuum plasma model as elucidated by Su and Lam (1963) for quiescent plasma ($R_e < 1$) . It was soon realized though that the flowing plasma is the more common experimental continuum plasma simply from the methods of plasma generation. Examples of

flowing plasmas are MHD flows, flames, and argon arcs with respective flow speeds of 100 m s^{-1}, 5 m s^{-1} and 30 m s^{-1} (Clements et al., 1972). Lam (1964) studied the incompressible flow continuum plasma and soon afterward Su (1965) extended the study to compressible flow. These last two studies were limited to $\chi_p(\lambda_D/l)^2 << 1$ when the ion sheath is very thin. Stahl and Su (1971) obtained detailed current-voltage characteristics for flush mounted, highly negative probes with a thick one dimensional sheath. Dukowicz (1969, 1970) numerically solved the two dimensional Poisson's equation for highly negative probe potentials using flat plate and cone geometries.

There are four equations common to these previously mentioned probe theories though simplified conditions may reduce this number. First, there are the ion and electron conservation equations which account for charge species conservation and include production, recombination, convection, diffusion and mobility. When the electron and ion temperatures are not equal, the electron energy equation is required. Most theories do not involve themselves with the electron energy equation except when $\tilde{T}_-/\tilde{T}_+ = a\ constant$ and when $\tilde{T}_-/\tilde{T}_+ = 1$; thus the electron energy equation can be deleted. Finally, Poisson's equation must be satisfied. Together, these four equations are a set of elliptic equations which cannot be solved analytically except in simplified cases. A good review of the different approximate methods is given by Chung et al. (1975).

The most thorough study to date of the two dimensional plasma flow over a negatively biased flat plate has been done numerically by Russo and Touryan (1972) where they allowed for variable ion and

electron transport properties, nonequilibrium chemistry and differing ion and electron temperatures. Notable from Russo and Touryan's work is that they substantiated previous authors' analytical approximate methods of solving particular problems. Good agreement was found between Russo and Touryan's results and those of Stahl and Su (1971). Stahl and Su's method is extended in this thesis to include variable ion transport properties and nonequilibrium chemistry. Russo and Touryan concluded that the transport properties are crucial for the ion density profile and consequently the ion current density to the probe. For example, in the case of a cooled probe, an unexpected rise in the ion density near the sheath before going to zero at the probe surface was calculated. This phenomenon resulted from the decreased ion mobility and the reliance upon diffusion to maintain current continuity through the sheath. Russo and Touryan's work clearly pointed out that changing transport properties and the plasma nonequilibrium must be accounted for in every model attempting to describe the sheath structure and probe current-voltage characteristics.

In the approximate methods, one serious effort to account for ion and electron production inside the ion sheath was done by DeBoer et al. (1969) where convection brought ions to the ion sheath and they were collected by the probe through ion mobility inside the sheath. Though production was accounted for, the model was simplified by having an ion sheath that was thick compared to the viscous boundary layer and production was constant. A correction for viscous boundary layer effects was done by Johnson and DeBoer (1973) who allowed the ion mobility around a cooled flat plate to decrease following Langevin's

theory (see Loeb, 1961). The point that arises is that the models of the ion collection characteristics are either for the thick ion sheath extending into the freestream plasma flow so that the quasi-neutral plasma is unaffected by the viscous boundary layer (DeBoer, 1973) or alternatively, the ion sheath is thin so that it is inside the viscous boundary layer and either convection or diffusion is corrected in the ion transport to the probe (Lam, 1964; Su, 1965; Stahl and Su, 1971). When the ion sheath is slightly thinner than the viscous boundary layer, a correction is required for the convection of the ions to the ion sheath edge, ambipolar diffusion in the quasineutral region and ion mobility in the ion sheath. A gap in the approximate methods exists for this case of probe operation and will be filled by the theory in this thesis.

For the thick ion sheath at large potentials, a very useful approximate method had been developed by DeBoer (1968) and Clements and Smy (1970) where the ion flux convected to the sheath edge is equated to the space charge ion flux inside the sheath (see Cobine, 1958). No corrections for a viscous boundary layer are made nor are nonequilibrium chemistry effects considered. These corrections are not important when the ion sheath is very much thicker than the viscous boundary layer. This model also ignores the ambipolar diffusion in the thin quasineutral region. The value of the model is that it successfully predicts the current density to a planar probe operated in the thick sheath mode when convection dominates outside the sheath and provides a comparison for the more detailed models mentioned earlier.

Few flowing plasma models extend beyond a steady bias applied to the probe. Clements and Smy's (1970) model is amenable to a.c. transient response studies of the sheath edge motion (Smy, 1976). This possibility will be explored in the theory to develop a first order approximation to relaxation phenomena for the planar probe. Of the recent investigations of Langmuir probe responses to voltage transients, most were studying the current spike to a probe for a very large negative going voltage step. Thomas (1969) experimented with a cylindrical probe aligned perpendicular to the flame flow of a CsCl seeded Meker burner. By switching the probe from floating potential to -90 V, Thomas observed a current spike which relaxed in 1 ms for a 1 mm diameter probe and flow speed of 3 m s^{-1}. Subsequently, Clements and Smy (1970) confirmed Thomas' observations but extended the work to include a wide range of ion densities (10^{15} - 10^{18} m^{-3}), probe voltages (10 - 400 V) and flow velocities (5 - 40 m s^{-1}). Clements and Smy also offered a theory based on the space charge equation for a collision dominated plasma with $\mu_{+o} V_p / r_s >> dr_s/d\tilde{t} >> U_o$ where μ_{+o} is the ion mobility and r_s is the sheath thickness. These bounds on the sheath expansion velocity are limiting it to be larger than the plasma flow speed and smaller than the field impelled ion velocity inside the sheath. If $dr_s/d\tilde{t} > \mu_{+o} V_p / r_s$ then the ion transit time through the ion sheath must be considered (Rosa, 1971). The net current to the probe is equal to the charge uncovered by the expanding sheath as the electrons recede from the probe. Clements and Smy (1971) extend their cylindrical probe study to spherical geometry and predict a $\tilde{t}^{-\frac{1}{2}}$ response ($\tilde{t}$ is time) in the current spike. Oliver

and Clements (1975) slightly modify the theory of Clements and Smy (1971) to include the trailing edge of the spike where $dr_s/d\tilde{t} < U_o$.

Clements and Smy (1971) showed that for high sheath expansion velocities and $R << r_s$ the ion current to a spherical probe pulsed from floating potential to a negative voltage V_p behaved as

$$I_s = 2\pi(\varepsilon_o \mu_{+o} eN_o)^{\frac{1}{2}} RV_p \tilde{t}^{-\frac{1}{2}}$$

I_s is the probe current and R is the probe radius. Thus by observing the time dependent behaviour of the sphere's current, it is possible to deduce the ion density of a flowing plasma without any concern for the plasma flow speed. However, this and other work with the pulsed probe do not render the most information this technique has to offer. Both the probe geometry and probe bias conditions of Clements and Smy and other workers limited the pulsed probe method. By using cylindrical probes, the sheath expansion time can be recorded, but unless a second search probe is used to detect this sheath edge (Oliver and Clements, 1975) only an estimate of the sheath expansion speed can be made. By using a flat plate aligned parallel to the plasma flow, a different relaxation of the probe current occurs for a small change in the voltage. Here, it is conceivable that the ion sheath edge motion resulting from the voltage change can be slower than the flow velocity and the ion transit speed through the sheath, i.e. $\mu_{+o} V_p / Y_s >> U_o >> dY_s/d\tilde{t}$ where Y_s is the sheath thickness around the probe. The purpose of this operation is to have the flow speed dictate the relaxation time at any point downstream from the plate's leading edge. The change of the plasma characteristics due to the

voltage step, are swept by the neutral gas flow past a given point and detected as a change of the probe's current. When the sheath edge extends beyond any viscous or thermal boundary layer surrounding the plate, the relaxation time is not related to the sheath thickness as in the case of a porous flat plate aligned perpendicular to the plasma flow (Noor et al., 1977). Ion convection speeds to the ion sheath edge decrease if the probe bias conditions are such that the ion sheath is completely inside the viscous boundary layer. The result would be an increased relaxation time as the flow time to a point downstream is longer than in the freestream plasma. This possibility will be examined in this thesis and yields an electrical method of studying the hydrodynamic boundary layer around a flat plate in a weakly ionized flowing gas.

The remaining chapters of this thesis will concentrate on two problems mentioned here. First the general behaviour of the pulsed probe ion current will be derived in section 2.3. Following this derivation, the d.c. behaviour of the flat plate probe with the ion sheath edge inside the viscous boundary layer is examined. The purpose of the d.c. study is to predict the probe current relaxation time for a given voltage step in the probe's potential. The relaxation time can be calculated from the flow speed at the final position of the ion sheath edge. Chapter 3 outlines the experiments which were performed and Chapter 4 summarizes and comments on the results of the experiments. Conclusions on this work and suggestions of possible future lines of research are in Chapter 5. Dimensional quantities are in SI units unless noted otherwise.

CHAPTER 2

THEORY

2.1. General Discussion

It is of fundamental importance to understand what mechanisms are responsible for the ion and electron motion in the plasma surrounding a probe. There are three mechanisms of interest here. First, there is diffusion where a gradient in the ion or electron density results in diffusion of particles from regions of high density to those of low density. Secondly, there is charged particle mobility in any electric fields around the probe. Finally, if the plasma is flowing, convection of ions and electrons may be important. Lam (1964) considered plasma flow velocity and derived the following equation describing the ion density around an ion collecting flat plate probe ($\tilde{T}_+ = \tilde{T}_-$)

$$2\frac{\partial^2 n_+}{\partial \zeta^2} - \left(U\frac{\partial n_+}{\partial X} + vR_e \frac{\partial n_+}{\partial \zeta} \right) = R_e \alpha^2 \frac{\partial}{\partial \zeta}\left(\frac{\partial \chi}{\partial \zeta}\frac{\partial^2 \chi}{\partial \zeta^2} + \frac{\partial^3 \chi}{\partial \zeta^3} \right) \tag{2.1.1}$$

X and Y are directions parallel and perpendicular to the probe and U and v are the corresponding particle speeds. $\alpha = \lambda_D/l$; $\zeta = YR_e^{\frac{1}{2}}$; $\chi = eV/k\tilde{T}_{-o}$. The first term on the left side of Eq. (2.1.1) represents ion diffusion, the second term, ion convection and the right hand side is ion mobility. The order of the three terms are $O(1/\zeta^2)$, $O(1)$, and $O(R_e\alpha^2\chi^2/\zeta^4)$. Clements and Smy (1970) have shown for $R_e\alpha^2\chi^2 << 1$, the right hand side of Eq. (2.1.1)

may be neglected and the plasma around the probe is diffusion dominated with convection supplying the ions to the diffusion layer adjacent to the probe. When $R_e\alpha^2\chi^2 >> 1$, the first term on the left hand side of Eq. (2.1.1) is small and in this case convection supplies the ions to the ion sheath which are then moved to the probe by mobility in an electric field. Clements and Smy (1971) go further to show that for a flush mounted probe on a flat plate, the mobility effects dominate when $R_e\alpha^2\chi^2 > (b/l)^2$ where b is the flush probe downstream length. For $R_e\alpha^2\chi^2 \sim 1$, both diffusion and convection must be considered significant. In this case, the plasma around the probe may be divided into two regions. One region is closest to the probe where mobility is still dominant, and just outside this ion mobility region, diffusion and convection dominate in the ion transport. In this thesis, the case of $R_e\alpha^2\chi^2 << 1$ will not be studied, but rather, moderate probe potentials are studied where χ is large enough for mobility to be a controlling mechanism in the ion collection. The motivation for a large χ is more than just to ensure that the ions are transported by their mobility when close to the probe. If χ is small, then the electron flux will be significant in the net current collection which is undesirable since relaxation times are being studied. The electrons come to equilibrium after a change of the probe voltage in a time much shorter than the times associated with any convection from the flat probe's leading edge. If the monitored current is significantly electron collection, then very fast relaxation times result and do not relate to the plasma flow speed.

2.2. Probe Floating Potential

Though not of large theoretical interest in this thesis, the calculation of the floating potential is still of paramount importance in properly interpreting experimental results. As discussed in the Introduction and seen in Fig. 1.2, the floating potential is easily measured as the voltage where there is no net probe current. However, plasma potential is the zero potential because an object at this potential does not electrically disturb the plasma. Unfortunately, the plasma potential is often not easily measured without greatly perturbing the plasma and it is not likely that the plasma and floating potential are equal (unless $\tilde{T}_{\alpha o} = 0$). To circumvent this problem, the floating potential in a plasma model can be calculated by equating the random thermal electron flux to the probe, to the ion flux predicted by the model. The calculated floating potential gives the difference between it and the plasma potential which then allows the experiment's voltage measurements to be referenced to the plasma potential. Very simply then

$$V = \underset{(Theory)}{V_F} + \underset{(Experiment)}{V_{w.r.t.\ Floating\ Potential}} \tag{2.2.1}$$

Although, as Clements and Smy (1974) show, the calculation of the floating potential V_F in a collisional flowing plasma is not, in general, straightforward, the following simple approach is generally accurate enough. This is especially true for the present case where V_F is a relatively small correction to V .

From Chen (1965), the electron flux to the plate at floating potential V_F for a Maxwellian particle energy distribution is

$$j_- = \tfrac{1}{2} N_o e \left(\frac{2k\tilde{T}_-}{\pi m_-}\right)^{\frac{1}{2}} e^{-(eV_F/k\tilde{T}_-)} \tag{2.2.2}$$

The ion current can be approximated by the theory of Clements and Smy (1970) and DeBoer and Johnson (1968) to make the calculation tractable. Other more exact theories such as Russo and Touryan (1972), Johnson and DeBoer (1971) and Stahl and Su (1971) yield unwieldy numerical results and lead to only a small correction of Clements and Smy's current density calculations (Chung et al., 1975). From Clements and Smy (1970), the ion flux to a flat plate for $R_e \alpha^2 \chi^2 > 1$ is

$$j_+ = (9\varepsilon_o \mu_{+o} V_F^2)^{1/4} \left(\frac{eN_o U_o}{8X}\right)^{3/4} \tag{2.2.3}$$

Eqs. (2.2.2) and (2.2.3) are set equal to each other since the ion and electron currents are equal, and for given experimental parameters, V_F can be solved for by the Newton-Raphson method. Finally from Eq. (2.2.1), voltages in the experiment can be adjusted to be referenced to the plasma potential.

2.3. Sheath Relaxation with the Simple Model

The aim of this section is to devise a simplified model to explain the ion current characteristics of a flat plate to which a step voltage has been applied. The relaxation of the ion current is directly related

to the plasma flow velocity at the ion sheath's final equilibrium position. In a low ion density plasma, the ion sheath edge can be sufficiently thick so as to be far away from the viscous and thermal boundary layers adjacent to the plate. Here, the relaxation will characterize the freestream flow velocity and with $R_e\alpha^2\chi^2 >> 1$, the simplifying assumption of mobility dominated ion transport close to the probe can be made. Also, $R_e\alpha^2 < 1$ is assumed to ensure that the ion streamlines in the ion sheath are nearly perpendicular to the plane surface (Smy, 1976) and the current density at the probe surface is equal to the current density convected into the ion sheath. Clements and Smy (1970) and DeBoer and Johnson (1968) solved the probe characteristics for a steady state solution, while here the model is extended to a time dependent solution to predict the behaviour of flush probes measuring the ion current density to the flat plate. Thomas (1969), Clements and Smy (1970) and Oliver and Clements (1975) pulsed cylindrical probes aligned perpendicular to the plasma flow and studied characteristics for a rapidly expanding ion sheath. These studies were different from the work here since here the disturbance is flowing parallel to the probe surface and the relaxation time is a function of the distance downstream from the probe's leading edge. Also, for these earlier studies, convection was not important in the ion sheath formation but rather the ion mobility in the ion sheath. Fig. 2.1 illustrates the present situation in this model.

For large negative probe potentials, the electron density close to the plate can be approximated as zero (Su and Lam, 1963) and the space charge equation for a collisional plasma (Cobine, 1958) gives

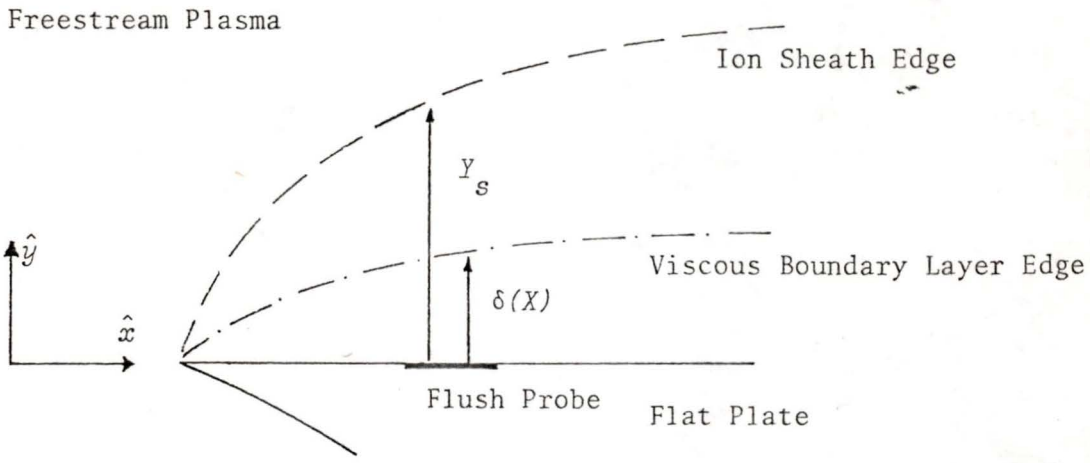

Figure 2.1. Diagram of Flat Plate Operation in a Low Ion Density Plasma

the ion current density to the plate as

$$j_+ = \frac{9\mu_{+o}\varepsilon_o V^2}{8Y_s^3} \tag{2.3.1}$$

Eq. 2.3.1 approximates the ion current flux to the flat plate as being ion mobility dominated in the ion sheath region and following Clements and Smy (1970), the voltage drop is taken to be entirely across the ion sheath region with no electric field extending beyond it. Again, with $R_e\alpha^2\chi^2 >> 1$, diffusion to the sheath edge can be neglected and

$$j_+ = N_o e \frac{\partial Y_s}{\partial \tilde{t}} + N_o e U_o \frac{\partial Y_s}{\partial X} \tag{2.3.2}$$

The first term on the right hand side of Eq. (2.3.2) is ion collection when the motion of the sheath sweeps into the undisturbed plasma resulting in more ions being impelled by the electric field towards the flat plate. $\partial Y_s/\partial\tilde{t} = 0$ is the condition of steady state where the plate voltage and current are unchanging. The second term of Eq. (2.3.2) is ion convection into the sheath with $\partial Y_s/\partial X$ being the slope of the ion sheath which is intercepting the ion flow in the freestream plasma. Once inside the ion sheath, the ions are mobility impelled towards the flat plate and the currents in Eqs. (2.3.1) and (2.3.2) can be equated

$$\frac{9}{8}\mu_{+o}\varepsilon_o \frac{V^2}{Y_s^3} = N_o e \left[\frac{\partial Y_s}{\partial \tilde{t}} + U_o \frac{\partial Y_s}{\partial X}\right] \tag{2.3.3}$$

For a step voltage applied to the flat plate at time $\tilde{t} = 0$, the voltage changes from V_i to V_f and Eq. (2.3.3) rewritten to include this time dependence becomes

$$\frac{9}{8}\mu_{+o}\varepsilon_o \frac{(V_i + H(t)(V_f - V_i))^2}{Y_s^3} = N_o e\left(\frac{\partial Y_s}{\partial \tilde{t}} + U_o \frac{\partial Y_s}{\partial X}\right) \qquad \begin{matrix} H(\tilde{t})=0 & t<0 \\ =1 & t\geq 0 \end{matrix} \tag{2.3.4}$$

For both $\tilde{t} < 0$, $\tilde{t} \to \infty$, $\partial Y_s/\partial \tilde{t} = 0$ and the result is familiar from Clements and Smy (1970) and DeBoer and Johnson (1968)

$$Y_s = \left(\frac{9\mu_{+o}\varepsilon_o V_i^2}{2N_o e U_o}\right)^{1/4} X^{1/4} \qquad \tilde{t} < 0 \tag{2.3.5}$$

$$Y_s = \left(\frac{9\mu_{+o}\varepsilon_o V_f^2}{2N_o e U_o}\right)^{1/4} X^{1/4} \qquad \tilde{t} \to \infty \tag{2.3.6}$$

Eq. (2.3.4) is solved by the method of characteristics for first order partial differential equations to give Y_s as a function of time and position X from the flat plate leading edge. Defining the constant

$$a_1 = \frac{9\mu_{+o}\varepsilon_o V_f^2}{8N_o e} \tag{2.3.7}$$

Then for $\tilde{t} > 0$, Eq. (2.3.4) can be written as

$$\frac{a_1}{Y_s^3} = \frac{\partial Y_s}{\partial \tilde{t}} + U_o \frac{\partial Y_s}{\partial X} \tag{2.3.8}$$

Which by the method of characteristics yields

$$\frac{d\tilde{t}}{1} = \frac{dX}{U_o} = \frac{dY_s}{\left(\frac{a_1}{Y_s^3}\right)} \tag{2.3.9}$$

The first equality of Eq. (2.3.9) gives

$$\tilde{t} = X/U_o + C_1 \tag{2.3.10}$$

Where C_1 is a constant. The second equality of Eq. (2.3.9) gives

$$C_2 = X/U_o - Y_s^4/4a_1 \tag{2.3.11}$$

Where C_2 is also a constant but because Eq. (2.3.3) is only first order, there can be only one free parameter so $C_2 = g(C_1) = g(\tilde{t} - X/U_o)$ where g is some function. With Eq. (2.3.11), this finally yields

$$Y_s = (4a_1)^{1/4}\left[\frac{X}{U_o} - g\left(\tilde{t} - \frac{X}{U_o}\right)\right]^{1/4} \tag{2.3.12}$$

To satisfy the boundary Eqs. (2.3.5) and (2.3.6)

$$g\left(\tilde{t} - \frac{X}{U_o}\right) = H\left(\frac{X}{U_o} - \tilde{t}\right)\left(1 - \frac{V_i^2}{V_f^2}\right)\left(\tilde{t} - \frac{X}{U_o}\right) \tag{2.3.13}$$

And as an end result Eq. (2.3.13) becomes

$$Y_s = \left(\frac{9\mu_{+o}\varepsilon_o}{2N_o e}\right)^{1/4} V_f^{1/2}\left[\frac{X}{U_o} + H\left(\frac{X}{U_o} - \tilde{t}\right)\left(1 - \frac{V_i^2}{V_f^2}\right)\left(\tilde{t} - \frac{X}{U_o}\right)\right]^{1/4} \qquad \tilde{t} \geq 0 \tag{2.3.14}$$

Eq. (2.3.14) can be interpreted as saying that the ion sheath thickness increases for increasing time until $\tilde{t} = X/U_o$ when steady equilibrium of the ion sheath position is attained. Substituting for Y_s into Eq. (2.3.1) gives the current density to the flush probe as

$$j_+ = \frac{N_o e(9\mu_{+o}\varepsilon_o/2N_o e)^{\frac{1}{4}}(V_i + H(\tilde{t})(V_f - V_i))^2}{4V_f^{3/2}(X/U_o + H(X/U_o - \tilde{t})(1 - V_i^2/V_f^2)(\tilde{t} - X/U_o))^{3/4}} \tag{2.3.15}$$

The essential features of Eq. (2.3.15) are, after the voltage step and before the disturbance disappears, the current has a $\tilde{t}^{-3/4}$ dependence and a current spike is observed. A parameter which tests the validity of Eq. (2.3.15) in an experiment is the ratio

$$\sigma = \frac{j_{\tilde{t}=0+} - j_{\tilde{t}=0-}}{j_{\tilde{t}=\infty} - j_{\tilde{t}=0-}} \tag{2.3.16}$$

$j_{\tilde{t}=0+}$, $j_{\tilde{t}=0-}$, $j_{\tilde{t}=\infty}$ are represented in Fig. 2.2.

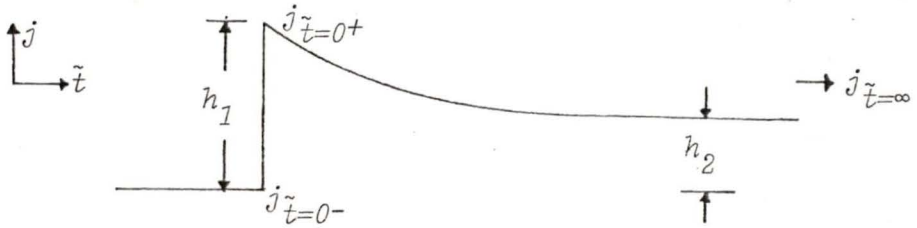

Figure 2.2. Diagram of the Probe Relaxation Current

By using Eq. (2.3.15), Eq. (2.3.16) can be evaluated and

$$\sigma = \frac{h_1}{h_2} = \{(V_f/V_i)^2 - 1\}/\{(V_f/V_i)^{\frac{1}{2}} - 1\} \tag{2.3.17}$$

When $V_f/V_i = 1 + \Delta$ where $0 < \Delta << 1$, σ can be written as $\{(1+\Delta)^2 - 1\}/\{(1+\Delta)^{\frac{1}{2}} - 1\}$ which to $O(\Delta)$ in a Taylor series expansion of the numerator and denominator gives $\sigma = 4$.

A significant correction to σ is evident from physical reasoning. Electron motion will be the only particle motion due to the voltage step in a time period of $O(Y_s^2/\mu_- V_i)$ This means that the electrons will recede from the plate to a new position Y_{fo} and the net density structure will be approximately the original ion density profile of the ion sheath to $Y_{s(\tilde{t}=0-)}$ and a net ion density of N_o between $Y_{s(\tilde{t}=0-)}$ and Y_{fo} . Beyond Y_{fo} , the plasma is quasineutral. The result of this change in the model is to decrease the mean electric field for the ion motion and to decrease the current spike to the probe. The electrons would recede in a period $O(10^{-7}$ s) and the current spike from their initial motion would not be resolvable from capacitive noise that is inherent from using a voltage step to create the plasma disturbance. The ion current spike to the flush probe which is of interest here, would be after $\sim 10^{-7}$ s when the ion density changes with the new plate potential. Clements and Smy (1971) have done a similar analysis for a pulsed spherical probe and their method is extended here to the flat plate probe.

An estimate of the correction to σ can be made by estimating Y_{fo} and using Y_{fo} to calculate a new $j_{\tilde{t}=0+}$ to substitute into Eq. (2.3.16) and give a new σ value. This correction to σ will be denoted σ' .

Just after the voltage transition, to first order, the voltage across the region to $Y_{s(\tilde{t}=0-)}$ is still V_i and $V_f - V_i$ is the

potential across the region $Y_{s(\tilde{t}=0-)}$ to Y_{fo} . By using the one dimensional Poisson's equation, Y_{fo} can be estimated

$$\frac{\partial^2 V}{\partial Y^2} = \frac{-N_o}{\varepsilon_o} \qquad Y_{s(\tilde{t}=0-)} \leq Y < Y_{fo} \tag{2.3.18}$$

Eq. (2.3.18) can be integrated twice and imposing the boundary condition that the electric field beyond Y_{fo} is zero, then Y_{fo} is

$$Y_{fo} = Y_{s(\tilde{t}=0-)} + \{(V_f - V_i)2\varepsilon_o/N_o e\}^{\frac{1}{2}} \tag{2.3.19}$$

It is important to note that if the voltage does not changes, then $Y_{fo} = Y_{s(\tilde{t}=0-)}$. The space charge equation can then be used to estimate $j_{\tilde{t}=0+}$.

$$j_{\tilde{t}=0+} = \frac{9}{8}\mu_{+o}\varepsilon_o \frac{V_f^2}{Y_{fo}^3} \tag{2.3.20}$$

Substituting for $j_{\tilde{t}=0+}$ in (2.3.16) gives the σ' value as

$$\sigma' = \left(\frac{V_f^2}{(V_i^{2/3} + (8\varepsilon_o U_o/9\mu_{+o}N_o eX)^{1/4} V_i^{1/6}(V_f - V_i)^{\frac{1}{2}})^3} - 1 \right) / ((V_f/V_i)^{\frac{1}{2}} - 1) \tag{2.3.21}$$

By comparing Eq. (2.3.20) to Eq. (2.3.17), it is easily seen that the correction to the current spike decreases the σ value as expected from physical reasoning. It is also interesting to see that σ' has an X dependence resulting from the changing magnitude of $Y_{s(\tilde{t}=0-)} - Y_{fo}$. As X becomes large, the ion sheath is thick and the distance the electron edge recedes is comparatively very small,

resulting in a smaller correction to σ .

The observation of the peak current affords a simple verification of the model for the high bias operation of the flat plate. The purpose of this simple model is to assist in understanding the more difficult case to be developed in section 2.5 where the ion sheath is inside a viscous boundary layer. The current characteristics for the ion sheath inside the viscous boundary layer can be expected qualitatively to be the same as for the simple model here. The initial current spike is an effect from the sheath thickness suddenly increasing and consequently the $\partial Y_s/\partial X$ term in Eq. (2.3.2) is increasing as well as $\partial Y_s/\partial \tilde{t}$ being a new term in the ion collection. For large V_f/V_i , the model cannot be expected to hold because the sheath will be expanding at speeds such that a nonequilibrium plasma inside the ion sheath results. The ion transit speeds in the ion sheath will then be much slower than the expanding sheath (Rosa, 1971) which quickly leads to nonlinear effects, the essential feature being that σ could be less than predicted. This simple model was developed with the implicit assumption that the ions traversed the ion sheath in zero time. However, when the sheath edge is moving faster than the ions, this approximation can no longer be made. No study of this problem has been done to date although Thomas (1969), Clements and Smy (1970) and Smy (1976) have recognized the limitations in the time resolution of an ion collecting probe, as in this case, when a large step voltage is applied to the probe.

2.4. Viscous and Thermal Boundary Layers Around a Flat Plate

For high ionization density and moderate probe bias, the ion sheath edge may be inside the viscous and thermal boundary layers (Smy and Noor, 1976). If this occurs, then the relaxation time of the ion current to the probe when applying a voltage step, can be expected to be longer than when the ion sheath edge is outside the viscous boundary layer. This latter case was studied in section 2.3. To estimate the relaxation time for the more complex case, the velocity structure of the viscous boundary needs to be elucidated.

Two important assumptions are that the flowing gas is weakly ionized so the hydrodynamic flow properties will be decoupled from the electric field and the plate temperature is assumed a constant over the whole surface. Polhausens' (1921) approximation of the velocity profile over a flat surface will be used where

$$\frac{U}{U_o} = 2\eta - 2\eta^3 + \eta^4 \qquad 0 \leq \eta \leq 1 \tag{2.4.1}$$

$\eta = Y/\delta_v(X)$ and $\delta_v(X)$ is the viscous boundary layer thickness a distance X from the leading edge. Von Karman's momentum integral equation for compressible flow is used for estimating $\delta_v(X)$. The steady two dimensional flow momentum equation (Stewartson, 1964) is

$$\rho U \frac{\partial U}{\partial X} + \rho v \frac{\partial U}{\partial Y} = \rho_o U_o \frac{dU_o}{dX} + \frac{\partial}{\partial Y}\left(\mu \frac{\partial U}{\partial Y}\right) \tag{2.4.2}$$

ρ is the mass density of the gas and μ is the viscosity. For the simple case of uniform freestream flow, the first term on the right hand side of Eq. (2.4.2) vanishes and the equation can be in-

tegrated from $Y = 0$ to $Y = h$ where h is some distance away from the flat plate

$$\int_0^h \rho U \frac{\partial U}{\partial X}\, Y + \int_0^h \rho v \frac{\partial U}{\partial Y}\, Y = \mu \frac{\partial U}{\partial Y}\Bigg|_0^h \tag{2.4.3}$$

Using the continuity equation $\nabla\cdot(\rho\underline{U}) = 0$, the second term on the left hand side of Eq. (2.4.3) can be integrated by parts and the equation changes to

$$\int_0^h \rho U \frac{\partial U}{\partial X}\, dY + \rho v(U - U_o)\Big|_0^h + \int_0^h (U - U_o)\frac{\partial}{\partial X}(\rho U)\, dY = \mu \frac{\partial U}{\partial Y}\Big|_0^h \tag{2.4.4}$$

As $h \to \infty$, the second term on the left hand side vanishes since $v = 0$ at $Y = 0$ and $U = U_o$ at $Y = \infty$. Also $\partial U/\partial Y \to 0$ as $Y \to \infty$ since this is now the freestream region and the equation simplifies to

$$\int_0^\infty \rho U \frac{\partial U}{\partial X}\, dY + \int_0^\infty (U - U_o)\frac{\partial}{\partial X}(\rho U)\, dY = -\mu \frac{\partial U}{\partial Y}\Big|_{Y=0} \tag{2.4.5}$$

Upon grouping terms on the left hand side of Eq. (2.4.5)

$$\frac{\partial}{\partial X}\int_0^\infty (\rho U^2 - \rho U U_o)\, dY = -\mu \frac{\partial U}{\partial Y}\Big|_{Y=0} \tag{2.4.6}$$

Before Eq. (2.4.6) can be solved, the thermal boundary layer around the plate needs to be known. The plate is cooled and maintained at a temperature $\tilde{T}_w$ such that $\tilde{T}_w < \tilde{T}_o$. $\tilde{T}_o$ is the freestream flow temperature. From thermal boundary layer theory as discussed

by Schlicting (1968), $\delta_{thermal}/\delta_v \sim 1/\sqrt{P}$ where $\delta_{thermal}$ is the thermal boundary layer thickness and P is the Prandtl number (P is the ratio of kinematic viscosity to thermal diffusivity). For air, the Prandtl number is slightly less than 1, but to good approximation, P can be taken as 1 (Schlicting, 1968) and the thermal and velocity boundary layers are of the same thickness. $\delta(X)$ will denote the thickness of these two layers. For subsonic gas flows, the temperature and velocity profiles are similar and for the cooled plate

$$\frac{\tilde{T} - \tilde{T}_w}{\tilde{T}_o - \tilde{T}_w} = \frac{U}{U_o} \tag{2.4.7}$$

Using the ideal gas law and Eq. (2.4.7), the density distribution inside the thermal boundary layer is

$$\rho = \frac{\rho_o}{(U/U_o)(1 - \tilde{T}_w/\tilde{T}_o) + \tilde{T}_w/\tilde{T}_o} \tag{2.4.8}$$

And defining $\tilde{T}_w/\tilde{T}_o = \nu$, then Eq. (2.4.6) becomes

$$\rho_o U_o^2 \frac{\partial}{\partial X}\int_0^\infty \left(1 - \frac{U}{U_o}\right)\frac{U/U_o}{((1-\nu)U/U_o + \nu)}dY = \mu U_o \frac{\partial}{\partial Y}\left(\frac{U}{U_o}\right)\Bigg|_{Y=0} \tag{2.4.9}$$

Upon changing variables in Eq. (2.4.9), the Polhausen velocity profile can be substituted and the left hand side of Eq. (2.4.9) integrated over η , $0 < \eta \leq 1$ (only integrating to $\eta = 1$ because the integrand vanishes for $\eta > 1$). Two integrals result

$$I_1 = \int_0^1 \frac{2\eta - 2\eta^3 + \eta^4}{(1-\nu)(2\eta - 2\eta^3 + \eta^4) + \nu} \, d\eta \tag{2.4.10}$$

$$I_2 = \int_0^1 \frac{(2\eta - 2\eta^3 + \eta^4)^2}{(1-\nu)(2\eta - 2\eta^3 + \eta^4) + \nu} \, d\eta \tag{2.4.11}$$

With these two integrals, Eq. (2.4.9) can be rewritten as

$$\rho_o U_o^2 (I_1 - I_2) \frac{d\delta(X)}{dX} = \frac{2U_o \mu_w}{\delta(X)} \tag{2.4.12}$$

The integration of Eq.(2.4.12) immediately yields the thickness of the viscous boundary layer as being

$$\delta(X) = \{4\mu_w X / ((I_1 - I_2)\rho_o U_o)\}^{\frac{1}{2}} = a X^{\frac{1}{2}} \tag{2.4.13}$$

This approximation of the boundary layer thickness for the gas flow over a cooled plate is used with Eqs. (2.4.1) and (2.4.7) to specify the thermal and viscous boundary layers around the flat plate. In the flowing plasma, these boundary layers will change the ion transport properties and the d.c. current characteristics of a conductor can be expected to differ from the predictions using the simple sheath model of section 2.3. In section 2.5, the d.c. case of the ion sheath completely inside the viscous boundary layer is studied and uses the results of this section.

2.5. Theory of the Ion Sheath Edge inside the Viscous Boundary Layer

2.5.1. Formulation of the Problem

The simple sheath model of section 2.3 demonstrated the relaxation of the ion sheath upon applying a step voltage to the flat plate in a flowing plasma. In section 2.4, the thermal and viscous boundary layer structure around the flat plate in the flowing gas was studied. Here, a more complicated approach to the ion collection is examined with the ion sheath inside the viscous and thermal boundary layers of the neutral gas flow. Inside the viscous boundary layer, the ion convection to the sheath edge will be reduced and at the same time, the ion transport coefficients for the mobility and diffusion decrease. D.c. characteristics of the plate current density and ion sheath edge position for a given distance downstream of the leading edge, as a function of plate voltage will be derived. The relaxation time of a step voltage response will be the flow time from the plate's leading edge to the point of interest, only now the flow speed will be less than the freestream velocity. The method of solution for the ion sheath edge position as a function of voltage is similar to the method of Stahl and Su (1971) but here variable ion transport and recombination are allowed.

The plasma disturbed by the presence of the probe is divided into two regions; the ion sheath closest to the flat plate and the quasi-neutral region just adjacent to the ion sheath. This is illustrated in Fig. 2.3. In the quasineutral region, the ion and electron numbers

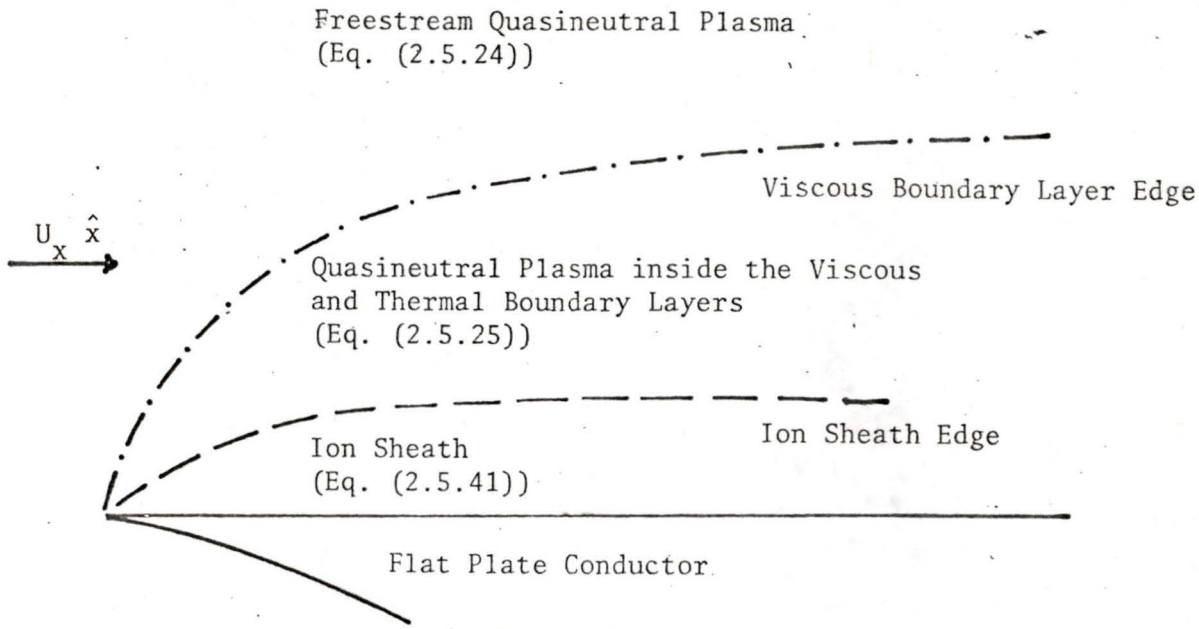

Figure 2.3. Ion Sheath Edge Inisde the Viscous Boundary Layer

are equal (Su and Lam, 1963) and the ion motion is governed by diffusion and convection. The ion sheath region has a predominance of ions and they are electric field impelled towards the flat plate. By matching the solutions of the quasineutral region and the ion sheath region, it is possible to get a complete solution to the sheath edge position and ion current density to the flat plate.

To begin with, the equations of continuity for the ions and electrons and Poisson's equation are

$$\frac{\partial N_+}{\partial \tilde{t}} + \nabla\cdot(\underline{U}N_+ + \underline{\Gamma}_+) = P_+$$

Ion Continuity (2.5.1)

$$\frac{\partial N_-}{\partial \tilde{t}} + \nabla\cdot(\underline{U}N_- + \underline{\Gamma}_-) = P_-$$

Electron Continuity (2.5.2)

$$\underline{\Gamma}_+ = -\tilde{D}_+\nabla N_+ - \frac{e\tilde{D}_+}{k\tilde{T}_+} N_+\nabla V$$

Ion Flux (2.5.3)

$$\underline{\Gamma}_- = -\tilde{D}_-\nabla N_- + \frac{e\tilde{D}_-}{k\tilde{T}_-} N_-\nabla V$$

Electron Flux (2.5.4)

$$\nabla^2 V = \frac{-e(N_+ - N_-)}{\varepsilon_o}$$

Poisson's Equation (2.5.5)

The first terms of Eqs. (2.5.1) and (2.5.2) represent recombination of the ions and electrons and the second terms represent convection, diffusion and mobility of the ions and electrons in the plasma.

The term on the right hand side of Eqs. (2.5.1) and (2.5.2) is the ion and electron production in the plasma. Eqs. (2.5.3) and (2.5.4) are the ion (electron) diffusion and ion (electron) mobility transport in the ion (electron) flux. $\tilde{D}_+$ and $\tilde{D}_-$ are the diffusion coefficients and the Einstein relation is used to write the mobility coefficient in terms of the diffusion coefficients. In their present forms, these equations are not very manageable and can be nondimensionalized to facilitate a study of them. The following equations define the dimensionless variables x , y , n_α , ϕ , u_x , u_y , D_α , T_α , and t .

$$X = lx \tag{2.5.6}$$

$$Y = (l\tilde{D}_{+o}/U_o)^{\frac{1}{2}}\, y \tag{2.5.7}$$

$$N_\alpha = N_o\, n_\alpha \qquad \alpha = + \text{ or } - \tag{2.5.8}$$

$$V = (k\tilde{T}_{+o}/e)\, \phi \tag{2.5.9}$$

$$U_x = U_o\, u_x \tag{2.5.10}$$

$$U_y = U_o(\tilde{D}_{+o}/U_o l)^{\frac{1}{2}}\, u_y \tag{2.5.11}$$

$$\tilde{D}_\alpha = \tilde{D}_o\, D_\alpha \qquad \alpha = + \text{ or } - \tag{2.5.12}$$

$$\tilde{T}_\alpha = \tilde{T}_{\alpha o}\, T_\alpha \qquad \alpha = + \text{ or } - \tag{2.5.13}$$

$$\tilde{t} = (l/U_o)\, t \tag{2.5.14}$$

The dimensional variables in Eqs. (2.5.1) to (2.5.5) can be eliminated to yield dimensionless variables in each term. Using Eq. (2.5.3)

to eliminate $\underline{\Gamma}_+$ in Eq. (2.5.1), the dimensionless ion continuity equation becomes

$$\frac{\partial}{\partial x}(u_x n_+) - \frac{\tilde{D}_{+o}}{U_o l}\frac{\partial}{\partial x}\left[D_+\left(\frac{\partial n_+}{\partial x} + \frac{n_+}{T_+}\frac{\partial \phi}{\partial x}\right)\right] + \frac{\partial}{\partial y}(u_y n_+)$$

$$- \frac{\partial}{\partial y}\left[D_+\left(\frac{\partial n_+}{\partial y} + \frac{n_+}{T_+}\frac{\partial \phi}{\partial y}\right)\right] = P_+ - \frac{\partial n_+}{\partial t} \tag{2.5.15}$$

Similarly for the electrons, Eq. (2.5.4) can be used to eliminate $\underline{\Gamma}_-$ in Eq. (2.5.2) to give the electron continuity as

$$\frac{\partial}{\partial x}(u_x n_-) - \frac{\tilde{D}_{-o}}{\tilde{D}_{+o}}\frac{\tilde{D}_{+o}}{U_o l}\frac{\partial}{\partial x}\left[D_-\left(\frac{\partial n_-}{x} - \frac{n_-}{T_-}\frac{\partial \phi}{\partial x}\right)\right] + \frac{\partial}{\partial y}(u_y n_-)$$

$$- \frac{\tilde{D}_{-o}}{\tilde{D}_{+o}}\frac{\partial}{\partial y}\left[D_-\left(\frac{\partial n_-}{\partial y} - \frac{n_-}{T_-}\frac{\partial \phi}{\partial y}\right)\right] = P_- - \frac{\partial n_-}{\partial t} \tag{2.5.16}$$

The two preceding equations are solved by analysing the quasineutral and ion sheath regions and applying the simplifying conditions in each case. The quasineutral region is macroscopically neutral with a weak electric field making ambipolar diffusion important in the ion transport (Chung et al., 1975). The solution of the quasineutral region will provide boundary conditions for the ion sheath region and the solution to the ion sheath region assumes large ion mobility effects and the electron density can be approximated as zero (or decreasing exponentially as in Lam (1964) and Su and Lam (1963)). The two regions in the plasma are studied separately.

2.5.2. Solution of the Quasineutral Region

To study the quasineutral region, Eqs. (2.5.15) and (2.5.16) can be merged into a single equation. The Electric Reynolds number $R_e = U_o \tilde{l}/\tilde{D}_{+o} >> 1$ is assumed which matches with the parameters in the experiment. This condition on R_e allows the deletion of the second term in Eqs. (2.5.15) and (2.5.16). Diffusion in the quasineutral region is ambipolar and the ambipolar diffusion coefficient is denoted $\tilde{D}_a$. Thus, the nondimensionalizing constants $\tilde{D}_{-o}$ and $\tilde{D}_{+o}$ in Eqs. (2.5.15) and (2.5.16) are changed to $\tilde{D}_a$ and then adding these two equations being aware that $n_+ = n_- = n$, gives

$$\nabla\cdot(\underline{u}n) + \left(\frac{\partial n}{\partial t} - P_+\right) - \frac{\partial}{\partial y}\left(D_+ \frac{\partial n}{\partial y}\right) = 0 \tag{2.5.17}$$

$D_+/T_+ = D_-/T_-$ was assumed and can be demonstrated by the use of Langevin's theory of charged particle mobility (Loeb, 1961). From Langevin's theory, if μ_α (α = + or -) denotes the mobility of the charged particles, $\mu_\alpha = \mu_{\alpha o}\rho_o/\rho$ where ρ is the mass density of the bulk gas and $\mu_{\alpha o}$ is the charged particle's mobility at a density ρ_o. The Einstein relation for sufficiently weak electric fields is $\tilde{D}_\alpha = \mu_\alpha k\tilde{T}_\alpha/e$ and coupled with Langevin's relation

$$\tilde{D}_{\alpha o} D_\alpha = \rho_o k\tilde{T}_{\alpha o} T_\alpha/\rho e \qquad \text{or}$$

$$D_\alpha = \frac{\rho_o}{\rho} T_\alpha = T_\alpha^2 \tag{2.5.18}$$

A more detailed treatment of this relation is given by Bradley and

Abrahim (1974). In a collisional plasma for weak electric fields, $T_- \simeq T_+$ so the assumption of $D_+/T_+ = D_-/T_-$ (remembering this equation is dimensionless) is a safe one. Section 2.4 on the velocity and temperature profiles gave

$$\begin{aligned} U &= U_o\, u\{Y/\delta(X)\}\, \hat{x} && Y < \delta(X) \\ &= U_o\, \hat{x} && Y \geq \delta(X) \end{aligned} \tag{2.5.19}$$

where $\delta(X) = aX^{\frac{1}{2}}$. Nondimensionalizing the equations for the velocity profile by defining a new constant

$$\beta = (\tilde{D}_{ao}/U_o a^2)^{\frac{1}{2}} \tag{2.5.20}$$

and a new variable

$$\gamma = y/x^{\frac{1}{2}} \tag{2.5.21}$$

the velocity profile around the plate is

$$\begin{aligned} u_x &= u(\beta\gamma) && \gamma < 1/\beta \\ &= 1 && \gamma \geq 1/\beta \end{aligned} \tag{2.5.22}$$

Analagous to the use of the similarity variable for fluid mechanics, the ion and electron number densities are assumed functions of γ (Stahl and Su, 1971). In the region of the disturbed plasma around the probe, there is a rapid change of n in the y direction as compared to the change of n in the x direction (Russo and Touryan, 1972; Stahl and Su, 1971; DeBoer and Johnson, 1971). Changing the derivatives to explicit γ dependence, the partial derivatives are

changed to

$$\frac{\partial}{\partial y} = \frac{1}{\sqrt{x}} \frac{d}{d\gamma} \quad ; \quad \frac{\partial}{\partial x} = -\frac{1}{2x} \gamma \frac{d}{d\gamma} \tag{2.5.23}$$

From this, Eq. (2.5.17) becomes

$$\frac{\gamma}{2} \frac{dn}{d\gamma} + \frac{d^2 n}{d\gamma^2} = 0 \qquad \gamma \geq 1/\beta \tag{2.5.24}$$

$$-\frac{\gamma}{2} \frac{d}{d\gamma}(un) - \frac{d}{d\gamma}\left[D_+ \frac{dn}{d\gamma}\right] + \frac{x}{2}\left[\frac{dn}{dt} - P_+\right] = 0 \qquad \gamma < 1/\beta \tag{2.5.25}$$

The production and recombination of charged particles are equal in the equilibrium freestream plasma and so the last term of Eq. (2.5.25) is not present in Eq. (2.5.24) which describes the quasineutral region in the plasma outside the viscous boundary layer.

To close the set of equations for the quasineutral region, equations for u and D_+ are required and come from section 2.4. The Polhausen velocity profile Eq. (2.4.1) in the dimensionless variables is

$$U = 2(\beta\gamma) - 2(\beta\gamma)^3 + (\beta\gamma)^4 \qquad \gamma < 1/\beta$$

$$= 1 \qquad \gamma \geq 1/\beta \tag{2.5.26}$$

As $D_+ = T^2$, Eq. (2.4.7) can be used to substitute for T and the diffusion coefficient written in terms of the velocity profile is

$$D_+ = (\nu + (1-\nu)u)^2 \tag{2.5.27}$$

Eqs. (2.5.24) to (2.5.27) are a complete set of equations which describe the ion and electron density structure throughout the quasineutral region. To approach these equations, Eq. (2.5.24) which describes the quasineutral region outside the viscous and thermal boundary layers is first solved. Eq. (2.5.25) which describes the plasma where changing convection and diffusion occurs, is then solved using the boundary conditions of $n(1/\beta)$ and $n'(1/\beta)$ (' denotes differentiation with respect to γ) from the solution of Eq. (2.5.24). Fig. 2.3 illustrates the regions of solution.

Eq. (2.5.24) is solved with the boundary conditions at infinity $n(\infty) = 1$, $n'(\infty) = 0$ and is rearranged to yield

$$\frac{dn'}{d\gamma} = -\frac{\gamma}{2} n' \tag{2.5.28}$$

Solving for n' from above

$$n' = C \exp(-\gamma^2/4) \tag{2.5.29}$$

Where C is a constant and the boundary condition $n'(\infty) = 0$ is met. Eq. (2.5.29) can be integrated from ∞ to the viscous boundary layer edge

$$n(1/\beta) - 1 = C \int_{\infty}^{1/\beta} \exp(-\gamma^2/4)\, d\gamma \tag{2.5.30}$$

Defining $\zeta = \gamma/2$ and redefining the limits of the integral, Eq. (2.5.30) gives

$$n(1/\beta) - 1 = C\{2\int_0^{1/2\beta} \exp(-\zeta^2)\, d\zeta - \sqrt{\pi}\} \tag{2.5.31}$$

Rearranging Eq. (2.5.31) gives C in terms of $n(1/\beta)$, and this is substituted into Eq. (2.5.29)

$$n'(\gamma) = \frac{(n(1/\beta) - 1)\exp(-\gamma^2/4)}{2\int_0^{1/2\beta} \exp(-\zeta^2)\, d\zeta - \sqrt{\pi}} \tag{2.5.32}$$

This is the equation for the ion density gradient through the freestream plasma. The value of Eq. (2.5.32) is that it directly supplies $n'(1/\beta)$ when $1/\beta$ and $n(1/\beta)$ are specified. It is apparent from Eq. (2.5.20) that $1/\beta$ carries information about the thermal and viscous boundary layer thicknesses around the flat plate. Eq. (2.5.25) is a second order ordinary differential equation for $n(\gamma)$ inside the viscous boundary layer (x a constant) and to solve, $n(1/\beta)$ and $n'(1/\beta)$ are given by Eq. (2.5.32)

Eq. (2.5.25) can be simplified further by imposing $x \sim 1$ and the net ion production results from the competing processes of ion-electron production and their recombination. The freestream plasma will be assumed at equilibrium and the net production to be zero. Ashton and Hayhurst (1973) did a series of experiments with alkali metals ionized in flames on the temperature and particle production. From their results, in dimensionless form, the net ion production in the quasineutral region is

$$P_+ - \frac{\partial n}{\partial t} = \left.\frac{\partial n}{\partial t}\right|_{net} = K\left(T^{\frac{1}{2}} \exp\left(\frac{E\Phi_i}{k\tilde{T}_o}\left(1 - \frac{1}{T}\right)\right) - \frac{n^2}{T^2}\right) \tag{2.5.33}$$

Φ_i is the ionization potential of the alkali metal (4.33 V for potassium). The first term on the right hand side of Eq. (2.5.33) is the production of charged particles which increases with temperature while the second term is recombination of the ions and electrons by $M^+ + e^-$ M (M denotes the alkali atom) and equally apparent, recombination decreases with increasing temperature. $K = \ell N_o \alpha_r / U_o$ where α_r is the recombination coefficient and the remaining factors are a result of using dimensionless variable. Noor et al. (1977) found for an air propane flame seeded with potassium $\alpha_r = 8 \times 10^{-15}$ m^3 s^{-1} at 1500^o k and for the remaining parameters, $K \sim 1$. Eq. (2.5.33) is completely specified and substituting it into Eq. (2.5.25) then exapanding all the derivatives, the quasineutral solution is described by the equation

$$-\frac{\gamma}{2}\frac{du}{d\gamma} n - \frac{\gamma}{2}\frac{dn}{d\gamma} u - \frac{dD}{d\gamma}\frac{dn}{d\gamma} - D\frac{d^2n}{d\gamma^2}$$

$$+ \frac{K}{2}\left(-T^{\frac{1}{2}} \exp\left(\frac{e\Phi_i}{k\tilde{T}_o}(1 - 1/T)\right) + \frac{n^2}{T^2}\right) = 0 \tag{2.5.34}$$

This equation is solved for n and $dn/d\gamma$ using a Runge-Kutta method of $O(h^4)$ (Greenspan, 1973) to where $n = 0$ and the value of γ at $n = 0$ specifies the ion sheath edge position. This condition for the ion sheath edge position is reasonable because of the low ion density inside the ion sheath and for high probe biases, the electron

density in the sheath can be approximated as being zero (Clements and Smy, 1969; Su and Lam, 1963; Stahl and Su, 1971). The matching of the solution of Eq.(2.5.34) to the ion sheath solution is effected by equating the ion current density which represents ion flux conservation when going from one region of the plasma to the other. Eq. (2.5.34) demonstrates a useful feature of nondimensionalizing the equation in that except for K , the freestream ion density and position downstream from the flat plate's leading edge are in the scaling factors. Only changes in the viscous and thermal boundary layers alter the solution as these changes manifest themselves in new boundary conditions from Eq. (2.5.32). Solving Eq. (2.5.34) and matching with the ion sheath solution to be derived soon, needs to be done for only one ion density and position downstream from the leading edge; appropriate use of the scaling factors can extend the solution in the applicable range of the theory. More will be said of this treatment of the solution after studying the ion sheath.

2.5.3. The Ion Sheath

The innermost plasma region adjacent to the flat plate is the ion sheath. Here, because of nonnegligible electric fields and different ion and electron densities, a new set of equations approximate the region. For a moderate bias on the flat plate, i.e., $R_e \alpha^2 \chi^2 > 1$, mobility in an electric field is the important mechanism for ion collection (Clements and Smy, 1970; Su and Stahl, 1971). The following derivation is similar to what has been done by previous authors (Clements and

Smy, 1970; DeBoer and Johnson, 1968) only now variable transport properties are allowed. Neglecting convection in Eqs. (2.5.15) and (2.5.16) and for a small Electric Reynolds number

$$\frac{\partial}{\partial y}\left(D_+ \frac{\partial n_+}{\partial y} + \frac{D_+}{T} n_+ \frac{\partial \phi}{\partial y}\right) = 0 \qquad (2.5.35)$$

$$\frac{\partial}{\partial y}\left(D_+ \frac{\partial n_-}{\partial y} - \frac{D_+}{T} n_- \frac{\partial \phi}{\partial y}\right) = 0 \qquad (2.5.36)$$

At this point free diffusion coefficients $\tilde{D}_{-o}$ and $\tilde{D}_{+o}$ are used as the scaling factors because the ion and electron densities are no longer equal. Eq. (2.5.36) can be integrated once and the corresponding constant of integration is taken to be zero since it represents the electron current to the negatively biased probe. Also for large ϕ, as the mobility dominates over diffusion (Clements and Smy, 1970), Eq. (2.5.36) gives the result $n_- = 0$ in the ion sheath region. This result is a reasonable approximation to the exponential drop off of the electron density that Lam (1964) and Russo and Touryan (1972) predict in their simpler models of frozen chemistry plasmas. $n_- = 0$ justifies approximating the net charged particle production as zero since no recombination occurs where there are no free electrons. In the cooled plasma region, generation of ion-electron pairs is also very low because of the exponential temperature dependence of ionization as shown in Eq. (2.5.33). One consequence of no electrons in the ion sheath is that free diffusion definitely occurs in this region as opposed to the ambipolar diffusion in the quasineutral plasma. This

result substantiates using $\tilde{D}_{-o}$ and $\tilde{D}_{+o}$ for nondimensionalizing the ion sheath equations.

Similar treatment of Eq. (2.5.35), only now the ion current is not negligible, results in the equation

$$-\frac{D_+}{T} n_+ \frac{\partial \phi}{\partial y} = I_+ \tag{2.5.37}$$

$I_+ = D_+(\partial n/\partial \gamma)$ at the ion sheath edge as calculated from the quasineutral region Eq. (2.5.34) to ensure current continuity where there is no production nor recombination. The dimensionless Poisson's equation in the ion sheath is

$$\frac{U_o \lambda_D^{\,2}}{\tilde{D}_{+o} l} \frac{\partial^2 \phi}{\partial y^2} = -n_+ \tag{2.5.38}$$

Eliminating n_+ between Eqs. (2.5.37) and (2.5.38) will give the potential field distribution through the ion sheath region in a differential equation

$$\frac{\partial}{\partial y}\left(\frac{\partial \phi}{\partial y}\right)^2 = +2I_+ \frac{\tilde{D}_{+o} l}{U_o \lambda_D^{\,2}} \frac{T}{D_+} \tag{2.5.39}$$

As with Eq. (2.5.37) where the diffusion coefficient was approximated as $D = T^2$, from Eq. (2.5.18), Eq. (2.5.39) becomes

$$\frac{\partial}{\partial y}\left(\frac{\partial \phi}{\partial y}\right)^2 = \frac{S}{T} \qquad S = \frac{2I_+ \tilde{D}_{+o} l}{U_o \lambda_D^{\,2}} \tag{2.5.40}$$

Looking at a distance l down from the flat plate's leading edge,

$x = 1$, $T = \nu + (1-\nu)(2(\beta y) - 2(\beta y)^3 + (\beta y)^4)$ and as $\partial\phi/\partial y = 0$ at the sheath edge for a smooth matching to the quasineutral region, twice integrating Eq. (2.5.40) gives the plate potential

$$\phi = \int_0^{y_s} \left(\int_{\beta y}^{\beta y_s} \frac{S/\beta \, d\zeta}{\nu + (1-\nu)(2\zeta - 2\zeta^3 + \zeta^4)} \right)^{1/2} dy \qquad (2.5.41)$$

It is evident that this equation is coupled to the quasineutral region solution by two parameters. These are the sheath edge position y_s in the limits of the integration and the ion current density I_+ . Also, as the ion flux due to convection is neglected, for voltages sufficiently high to bring the sheath edge close to the viscous boundary layer edge, convection will be important and the currents could be higher than predicted here. At low voltages, diffusion in the ion sheath region is more significant than mobility and the model again fails. In the case of low voltages, the probe characteristics are best described by models first elucidated by Lam (1964) and Su (1965) particularly for probe voltages close to the floating potential where the electron current can no longer be neglected.

Eq. (2.5.41) can be simplified in the case where the thermal boundary layer is replaced with a uniformly reduced temperature A , $\tilde{T}_o > A > \tilde{T}_w$. The new result is

$$\phi = \frac{2}{3} \left(+ \frac{S}{A} \right)^{1/2} y_s^{3/2} \qquad (2.5.42)$$

The $y_s^{3/2}$ dependence is predicted by Lam (1964) and Stahl and Su (1971) for high probe potentials in their models. This dependence

is revealed in the present plasma model not from limiting the general solution to high potentials (this is already in the solution), but from assuming a uniform temperature around the plate. To solve Eq. (2.5.41), the parameters y_s and $(\partial n/\partial y)|_{y_s}$ from the quasineutral solution are required and the integration is effected by double integration using Simpson's Rule.

As alluded to at the end of the discussion on the quasineutral region, the scaling factors from nondimensionalizing the original Eqs. (2.5.1) to (2.5.5) are very useful. They allow the solution for the sheath edge position and flat plate current density as a function of voltage to extend over a wide range of freestream ion densities N_o and distances from the leading edge, l . There is no explicit dependence on N_o nor l in Eq. (2.5.32) or (2.5.34) (except for K of Eq. (2.5.34)), while for Eq.(2.5.41) these dimensional quantities appear as a factor in ϕ . Upon returning to dimensional quantities

$$Y_s = \left(\frac{l\tilde{D}_{ao}}{U_o}\right)^{\frac{1}{2}} y_s(\beta,\nu,K) = l^{\frac{1}{2}} f_1(\beta,\nu,K) \tag{2.5.43}$$

$$I_{dim} = eN_o\left(\frac{U_o\tilde{D}_{ao}}{l}\right)^{\frac{1}{2}} D(\beta,y_s)\frac{\partial n}{\partial y} = \frac{N_o}{l^{\frac{1}{2}}} f_2(\beta,\nu,K) \tag{2.5.44}$$

$$V = \frac{k\tilde{T}_{+o}}{e}\phi(N_o,l,\beta,\nu,n(1/\beta)) = (lN_o)^{\frac{1}{2}} f_3(\beta,\nu,n(1/\beta)) \tag{2.5.45}$$

f_1 , f_2 , and f_3 are evaluated numerically (see Appendix A) and the above expressions extend the solution to any combination of

N_o and l . There is the constraint that the extension does not approach probe potentials close to the floating potential, nor potentials high enough to take the ion sheath edge outside the viscous boundary layer. K depends on N_o but only weakly affects the solution for ϕ , y_s and the ion density gradient.

2.6. Propagation of the Plasma Disturbance

From section 2.5, the ion sheath position as a function of voltage is calculated when the sheath is inside the viscous and thermal boundary layers. These results can be applied to a time varying problem for the relaxation of the ion current density after a step in the probe voltage. The current density measurements with a flush probe can be interpreted to give information on the velocity profile inside the viscous boundary layer. As outlined in section 2.2 for the simplified model, the sheath edge is expected to relax in the flow time from the leading edge of the plate to the flush probe. If the ion sheath edge is close to being parallel to the flat plate surface, then the disturbance from the voltage step propagates from the leading edge along a streamline parallel to the plate. Fig. 2.4 illustrates this.

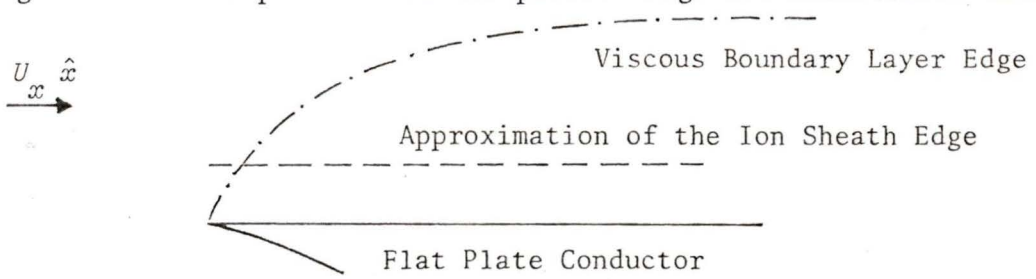

Figure 2.4. Approximation of the Ion Sheath Edge

From Eq. (2.5.22), the Polhausen velocity profile in the viscous boundary layer is

$$u_x = \frac{2\beta y}{x^{\frac{1}{2}}} - \frac{2(\beta y)^3}{x^{3/2}} + \frac{(\beta y)^4}{x^2} \tag{2.6.1}$$

$y = y_s$ and is a constant along the ion sheath edge and comes from the solution of the ion sheath edge position as a function of plate voltage. The velocity can be integrated from $x = 0$ to $x = 1$ and because of the normalization of x, the integration yields directly the average flow velocity from the leading edge to the point of interest

$$u_{average} = \int_0^1 u(x)\,dx = \int_0^{(\beta y_s)^2} 1\,dx + \int_{(\beta y_s)^2}^1 u_x(x)\,dx$$

$$= 4\beta y_s - 6(\beta y_s)^2 + 4(\beta y_s)^3 - (\beta y_s)^4 \tag{2.6.2}$$

The current spike produced during the voltage step will still be observed since the mechanisms of ion current collection are not radically different between the simple model and the corrected model of section 2.5. Coupled with the results of section 2.5, the average velocity to a given point downstream from the leading edge gives a strong tool for studying the nature of the plasma close to the flat plate. Monitoring current densities and relaxation times to flush probes mounted in the plate should enable measurements of the freestream ion density and the velocity structure of the viscous boundary layer. Refinements in the mathematical approach could be made but it is expected that as the underlying concepts are invariant, the corrections would not be large.

CHAPTER 3

EXPERIMENT

3.1. General Discussion

The relations between the different experimental procedures are important and are briefly summarized here. First, a cylindrical Langmuir probe made of thin platinum wire was used to measure the ion density structure of the low ionization flame. These measurements were important to ensure that anomalous ion density distributions resulting from the flame structure did not disturb the results compared with models which do not account for a nonuniform free-stream ion density. Preliminary to the plasma relaxation studies, the ion sheath formed on a negatively biased flat plate aligned parallel to the flame flow was detected using an air cooled spherical probe. A mapping of the thick sheath position as a function of plate voltage in a low ion density plasma was done with the spherical probe biased to be slightly electron collecting. Electron collection with the sensing probe is desirable to ensure that the resolution and sensitivity in finding the sheath edge would be limited by the sphere's size and not by difficulties in detecting the gradual changes in the ion currents as the spherical probe enters the sheath.

Electrical transients in the plasma were created by applying a step voltage to the flat plate and relaxation times of the disturbance were then measured. From previous theoretical considerations with

$R_e\alpha^2\chi^2 >> 1$, the relaxation time of the disturbance is equal to the distance downstream from the flat plate's leading edge, divided by the flame flow velocity. Experimentally demonstrating this effect is straightforward for a low ion density plasma ($N_o \sim 10^{15}$ m^{-3}) under thick sheath conditions, while the high ion density ($N_o \sim 10^{16}$ m^{-3}) requires the use of flush probes where there is a moderate sheath and $R_e\alpha^2 \sim 1$. The flush probe embedded in the flat plate allows flow velocities inside the viscous boundary layer of the plate to be measured. By changing the plate potential, the electric sheath can be positioned anywhere inside the viscous boundary layer and relaxation times of a transient disturbance will characterize the flow velocities at the final ion sheath position. The rest of the experimental section elaborates on the equipment and methods of each procedure discussed above.

3.2. Producing the Plasma

The flowing plasma used in this experiment was generated using a standard Meker burner supplied with a nearly stoichiometeric mixture of propane and air. Both the propane and air came from main outlets in the laboratory. For the case of the low ion density plasma, the H_3O^+ chemi-ions normally generated in the combustion process supply a sufficiently high ion density. The ion production is thought to be two step with $CH + O \rightarrow CHO^+ + e^-$, $CHO^+ + H_2O \rightarrow CO + H_3O^+$ (Bell et al., 1970; Miller, 1972). Though the actual ion production method suggested is not conclusively shown, the predominance of H_3O^+

in the flame is no longer in question. To achieve high ion densities, a specially constructed "seeder" with an aspirator was used to disperse a solution of KOH in water and the resulting mist was mixed with the normal air flow to the burner. The ion predominant in the seeded flame is the potassium since it has a low ionization potential, enabling high concentrations ($N_o \sim 10^{18}$ m^{-3}) of K^+ ions to be produced. The mechanism of ionization is $K + X \quad K^+ + e^- + X$ where X is a gas molecule colliding with the potassium with sufficient energy to ionize the potassium (Ashton and Hayhurst, 1973). By varying the potassium hydroxide concentration in the seeder, ion densities from 5×10^{16} m^{-3} to 5×10^{17} m^{-3} were possible.

The other important bulk characteristic of the plasma was its freestream flow velocity. Calculation of the flow velocity was done by measuring the air and propane flow to the burner and after combustion, the ideal gas law was used to calculate the volume flow rate. Knowing the burner top diameter as 3.7 cm, the flow velocity could be found. All experimental work was done with an air flow of 0.3 l s^{-1} and propane flow of 0.012 l s^{-1} (STP). Thus for a flame temperature of 1500^o K (measured using an optical pyrometer), the freestream flow velocity of 3.8 m s^{-1} was expected. These calculations do not consider possible entrainment of air into the flame and so are subject to some error. Measurements which are to be described later, used a spherical probe to give a corrected velocity which was then accepted as the plasma flow speed.

3.3. Probes

3.3.1. Cylindrical Probes

Ion density measurements for both the unseeded and seeded flames were done using cylindrical Langmuir probes of .25 mm diameter platinum wire which were passed through the flame at approximately 12 m s^{-1} using the rotating assembly shown in Fig. 3.1. The cylindrical probes were shielded with fine quartz tubing to allow localized plasma measurements and ensure that the measurements were not affected by the flame edge. When the cylindrical probe is negatively biased using a 30 V battery, the resulting probe current can be used to calculate the ion density using an empirical formula derived from microwave cavity ion density measurements (Clements and Smy, 1970)

$$N_o = 2.176 \times 10^{17} \, (I/(l_p v_f^{2/3}))^{1.23} \ \mathrm{m}^{-3} \qquad (3.3.1)$$

I is the probe current in μA , l_p is the probe length in cm and v_f is the probe speed relative to the plasma in m s^{-1}. Rapid fluctuations in the flame ionization produced disturbances large enough to make necessary an averaging of the current to the cylindrical probes to give an average ion density. Fig. 3.2 illustrates the averaging method. Essentially, the cylindrical probe current is converted from the low current signal (∿ 1 μA) to a voltage signal by using an operational amplifier. An integrator is gated to integrate only for the time the probe is passing through the flame. The time constant of the integrator is 1 s so typically for a period of rotation of 70 ms, the average of 15 current pulses of the cylindrical probe is taken and

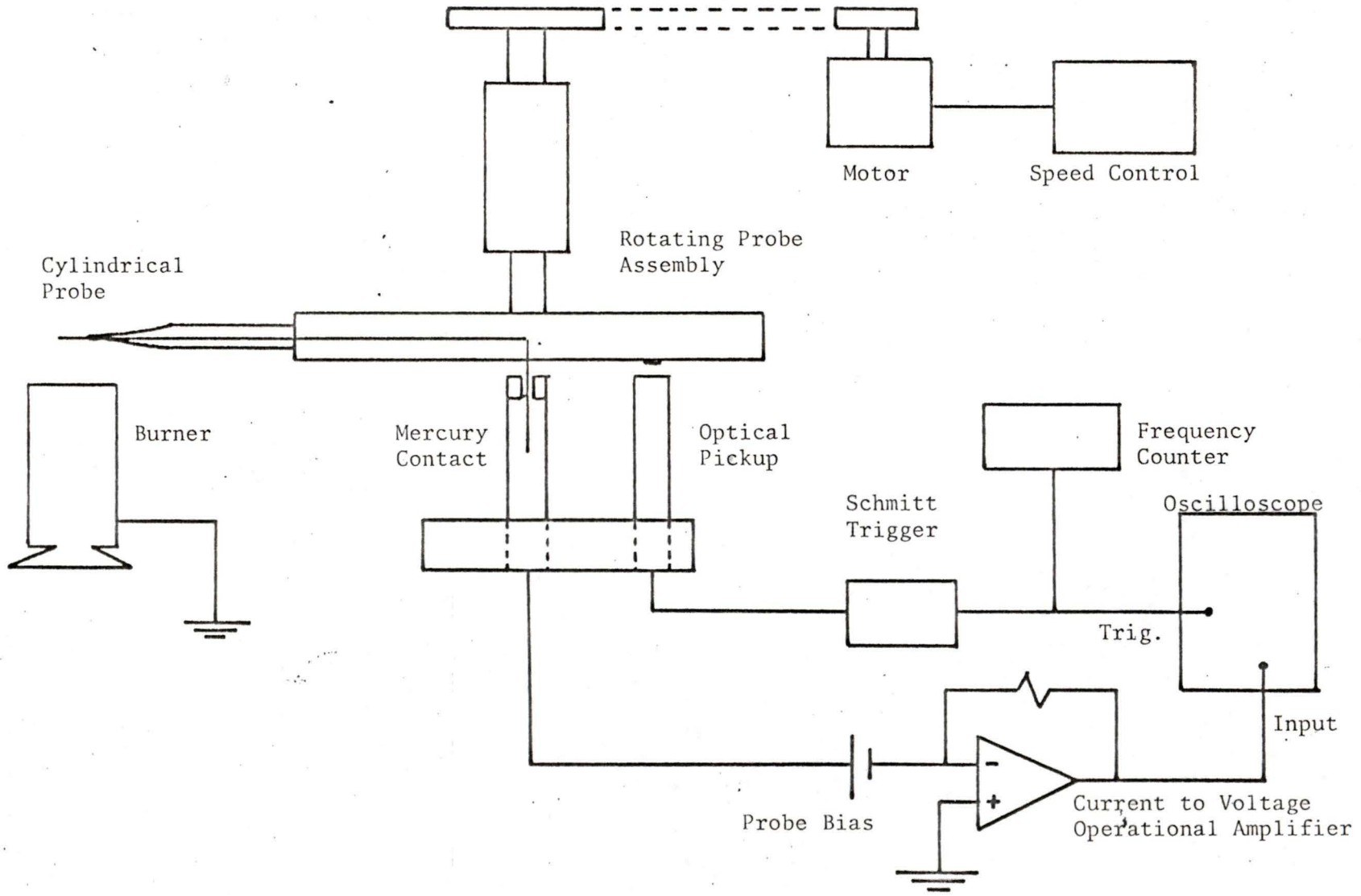

Figure 3.1. Apparatus for Measuring the Flame's Ion Density

outputted to an oscilloscope as a slowly varying d.c. signal. This method proved very reliable as a way of deducing the ion density.

3.3.2. Spherical Probe

Another probe used in the flat plate measurements was an air cooled spherical probe. Biased to be slightly electron collecting (voltage limited to $\sim +1$ V w.r.t. V_F or else the plasma may be strongly perturbed), the spherical probe was used to detect the ion sheath edge in the unseeded, low ion density flame. Biased at 30 V for ion collection, the spherical probe was also used to measure relaxation times for the same flame conditions. Fig. 3.3 illustrates the construction of the spherical probe. The probe was a 3.2 mm diameter bronze sphere with a 1 mm diameter air vent hole. The sphere was silver soldered to a 1.3 mm O.D. stainless steel tubing. The stainless steel tubing was co-axially shielded with quartz and stainless steel sleeves. The probe was mounted on an x-y mechanical stage to allow positioning of the probe any height above the burner and any distance from the flat plate. Downstream venting of the sphere's cooling air was done to ensure a mininum disturbance of the probe current and plasma structure around it. Work of Clements et al. (1977) and MacLatchy et al. (1974) on the current density to a spherical probe in a flowing plasma can be used for estimating the magnitude of the disturbance of the vented air. For a normalized current density I, $I = \cos^2 \theta/2$ was observed with θ being the azimuthal angle from the probe's stagnation point. In a worst case, imagining the vented air disturbing the

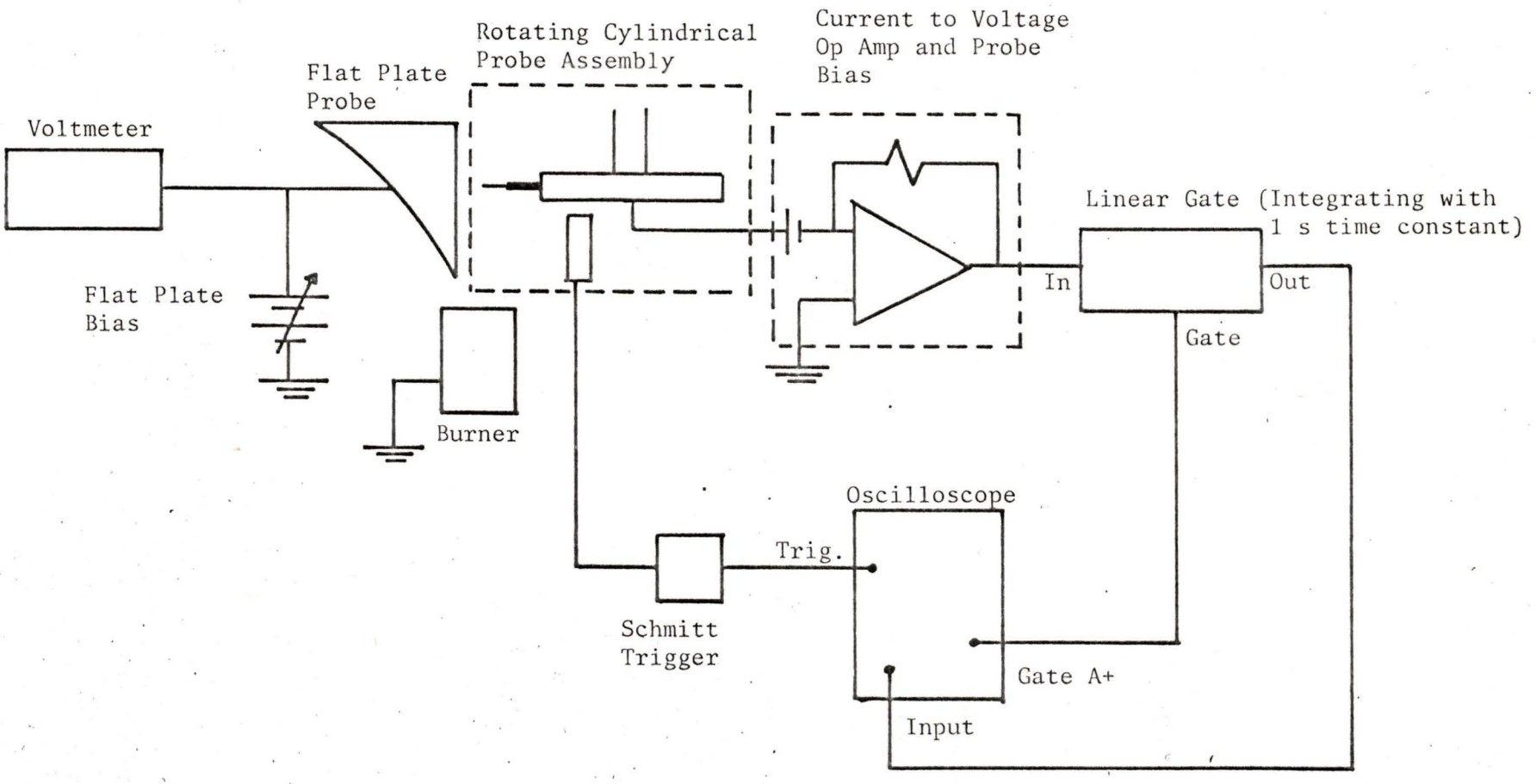

Figure 3.2. Circuit for Averaging the Cylindrical Probe Current

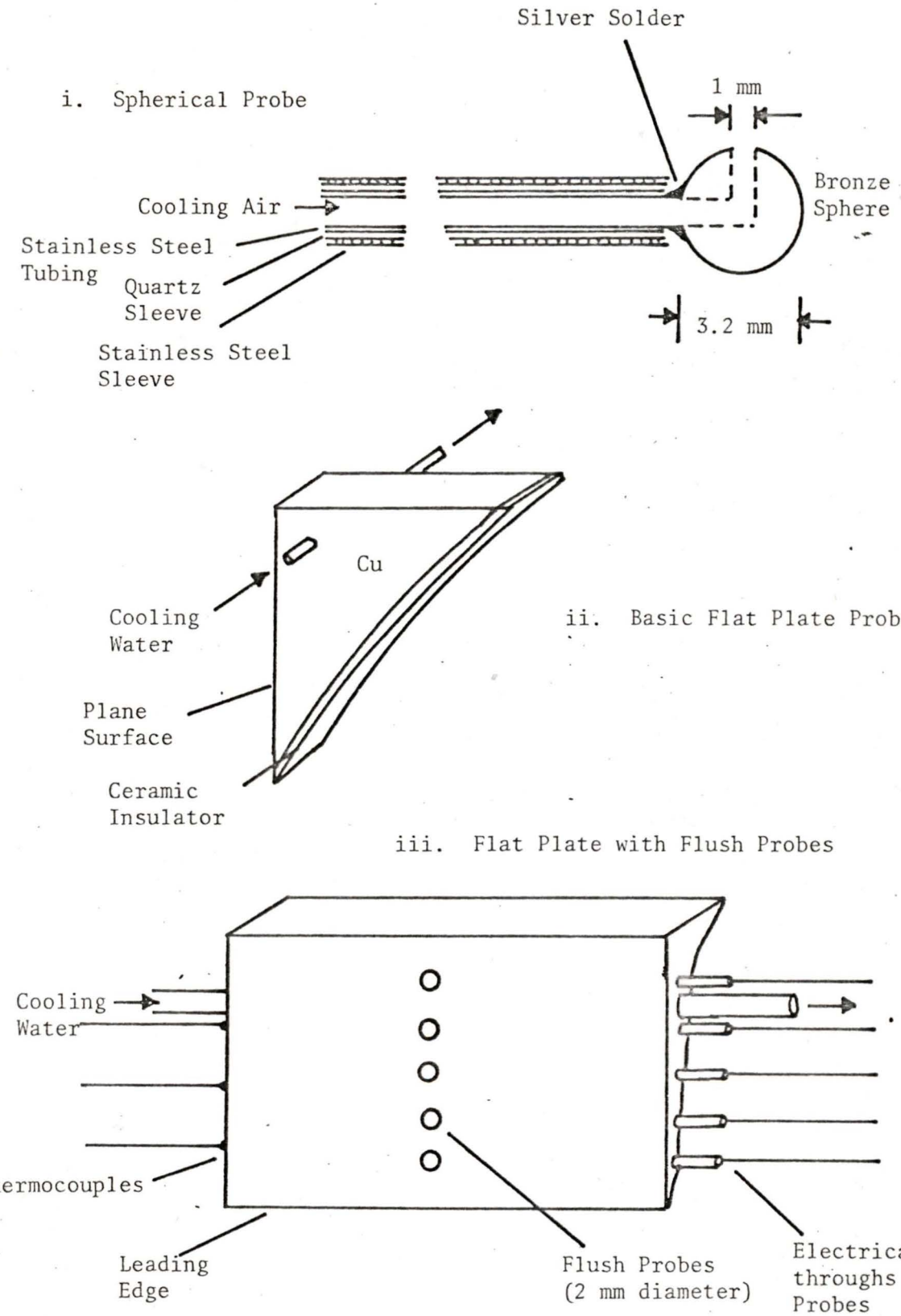

Figure 3.3. Construction of the Spherical and Flat Plate Probes

field flow from $\theta = \pi$ to $\theta = 3\pi/4$, the maximum current perturbation would be

$$\frac{\int_{3\pi/4}^{\pi} 2\pi R^2 \sin\theta \cos^2(\theta/2)\, d\theta}{\int_{0}^{\pi} 2\pi R^2 \sin\theta \cos^2(\theta/2)\, d\theta} \simeq 0.02 \qquad (3.2.1)$$

A 2% error is very small for the electron or ion current measurements where fluctuations in the flame parameters would make this effect unobservable.

3.3.3. Flat Plate Probe

The flat plate probe for the experiment was the flat side of a copper wedge aligned parallel with the flame flow. The copper wedge's leading edge was positioned 1 cm above the burner to make certain the wedge was above the flame's visible reaction zone which usually can extend approximately 5 mm to 10 mm above the burner. The wedges were made of copper to facilitate the water cooling that was necessary to prevent thermionic emission from the wedge and also to ensure the presence of a large temperature difference between the flame and copper to maximize the viscous and thermal boundary layer effects. Two copper wedges were constructed; one for the ion sheath position measurements using the spherical probe, while the second had flush probes for the ion current measurements. Electrical isolation of the first wedge was accomplished by installing showers (Sandhu and Weinberg, 1975) in the inflow and outflow cooling lines and electrically isolating the wedge from its support. The showers effectively dispersed the

cooling water into droplets to make certain the wedge would not be grounded by the water lines. The second wedge has a series of five 2 mm diameter copper flush probes, insulated from the main wedge with 1 mm thick mullite sleeves. These flush probes were arranged in line with the first one 1 cm downstream from the flat surface's leading edge and the successive probes spaced 1 cm apart. The construction of both wedges is illustrated in Fig. 3.3. Iron-constantan thermocouples were embedded in the side of the second wedge to monitor the wedge temperature throughout the experiment.

3.4. Experimental Procedure

The cylindrical probe discussed in section 3.3 was often used to determine ion densities for both high and low ion density plasmas. Measurements with the cylindrical probe were also used to determine ion density gradients in the plasma. Density gradients were seen as a change in the calculated ion density as the cylindrical probe was moved to sweep at different positions downstream from the flat plate's leading edge as well as different distances away from the plate. These gradients were then used to calculate the magnitude of ion diffusion and compare it with the ion convection in the plasma.

The method of using the spherical probe to detect the ion sheath around the flat plate is illustrated in Fig. 3.4. The wedge was biased strongly ion collecting and to eliminate possible supply voltage noise, a battery power supply was used. The spherical probe was biased slightly electron collecting (0.8 V w.r.t. V_F). The quick change

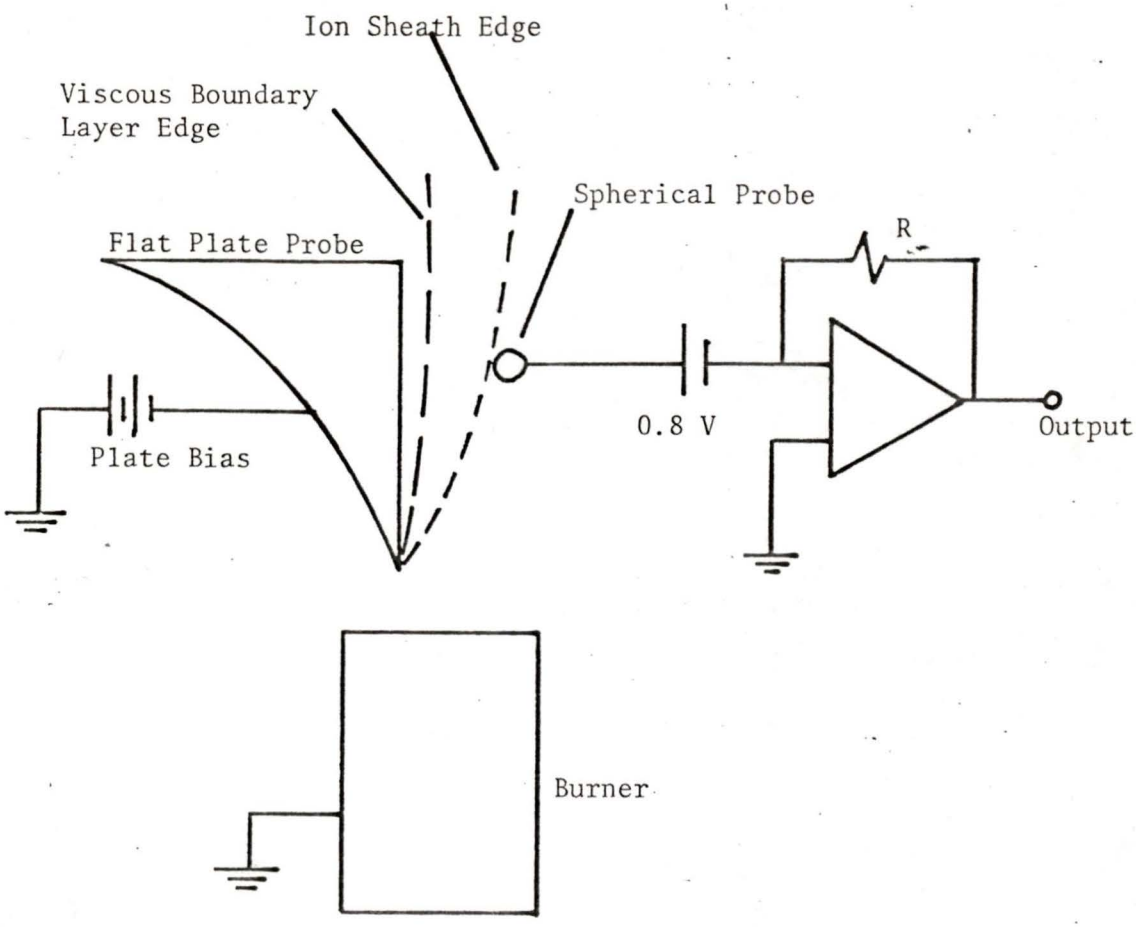

Figure 3.4. Method of using the Spherical Probe to detect The ion Sheath Edge

of electron density from the freestream value to practically zero inside the sheath gave a resolution in determining the ion sheath edge position limited only by the probe size. Following Oliver and Clements (1975), the sheath position was defined as the position where the electron current to the probe decreased by a factor of ½ from the freestream electron current measurements. The second part of the preliminary experimentation with the first flat probe was to measure the relaxation time of the sheath when a step voltage was applied to the probe. As explained in section 2.5, the increased voltage would move the ion sheath further out from the flat surface. The spherical probe was positioned inside the ion sheath before the step voltage was applied and was biased to be ion collecting (electron collection would be very low inside the ion sheath). Typically, spherical probe currents of 0.02 μA were measured and the flat plate was biased from 20 to 50 V with a step voltage change of 5 V to create the disturbance. The spherical probe could be moved to different distances from the leading edge of the plate to vary the relaxation time. The spherical probe was not used in the seeded, high ion density plasma for two reasons. First, the high ion density plasma required high voltages $\sim$ 200 V to create an ion sheath large enough to be able to surround the spherical probe. However, such high voltages can result in electrical breakdown inside the sheath (Nasser, 1971). Secondly, the potassium hydroxide quickly deposited on the spherical probe and disrupted the current measurements by shorting the sphere to the shield around the air supply tube (Clements, 1975).

Next, with the first flat plate assembly which had an insulated

side, the theory of the current spike to the probe when applying a voltage step was studied. These measurements were done for a low ion density plasma. By monitoring the total current to the flat plate, the current spike relaxation time was measured.

Having established the mechanism of the ion sheath relaxation, the second flat plate assembly with the flush probes was used to determine flow speeds in the viscous boundary layer adjacent to the plate. Because of capacitive coupling between the copper wedge and flush probes, it was not possible to apply a voltage step to the wedge and flush probe then measure the flush probe current separate from the total plate current. Thus, the flat plate assembly was grounded and the flush probes were connected directly to the operational amplifier input. A positive d.c. bias and positive going step pulse were applied to the Meker burner with the consequence of electron collection at the burner and ion collection again at the flat plate. Low ion density plasma measurements were not pursued beyond verification of the relaxation time previously measured using the first flat plate. High ion density in the plasma with moderate burner voltages gave an ion sheath thinner than the viscous boundary layer. A lower bound on the burner voltage came from needing to limit the electron current to the flush probe to very small values. When the voltage was not sufficiently electron retarding, the high mobility electrons had a short relaxation time through the ion sheath and would dominate the measurements. All five flush probe current densities were measured as a function of plate voltage and following Stahl and Su (1971) and Russo and Touryan (1972), a sudden change in the d.c. ion current

density indicated at what voltage the ion sheath was extending beyond the viscous boundary layer. This voltage put an upper bound on the voltage that would be useful to probe the viscous boundary layer velocity structure. Also, the average E/p values where E is the electric field in V m^{-1} and p is the gas pressure in Torr, could not be excessively large or Townsend discharge may occur (Nasser, 1971). The limiting E/p is $\sim$ 100 V m^{-1} $Torr^{-1}$ which for an atmospheric pressure plasma and for a typical ion sheath thickness of 2 mm for the seeded plasma, limits the applied voltage to < 150 V . The maximum voltages applied were below this value and during the experiment kept below 50 V.

The difficulty in the flush probe current measurements was fluctuations in the probe current caused by changes in ion density and flame speed. These fluctuations were as large as the step voltage response ($\sim 10^{-9}$ A) and had to be filtered and averaged out. The signal processing method is illustrated in Fig. 3.5 and explained as follows. The flush probe current is converted to a voltage signal using a low current offset operational amplifier in a current to voltage configuration. The voltage signal is filtered through a 10 KHz low pass filter (Krohn-Hite 3202, 6 db/octave) to remove high frequency components of the noise. After amplifying the filtered signal further, it is fed into a voltage controlled oscillator to create a frequency modulated pulse train. Using a linear gate (Brookdeal 415), this pulse train gates a triangle signal generator which is synchronous with the step voltage applied to the Meker burner. The result is a signal where time information is in the pulse height

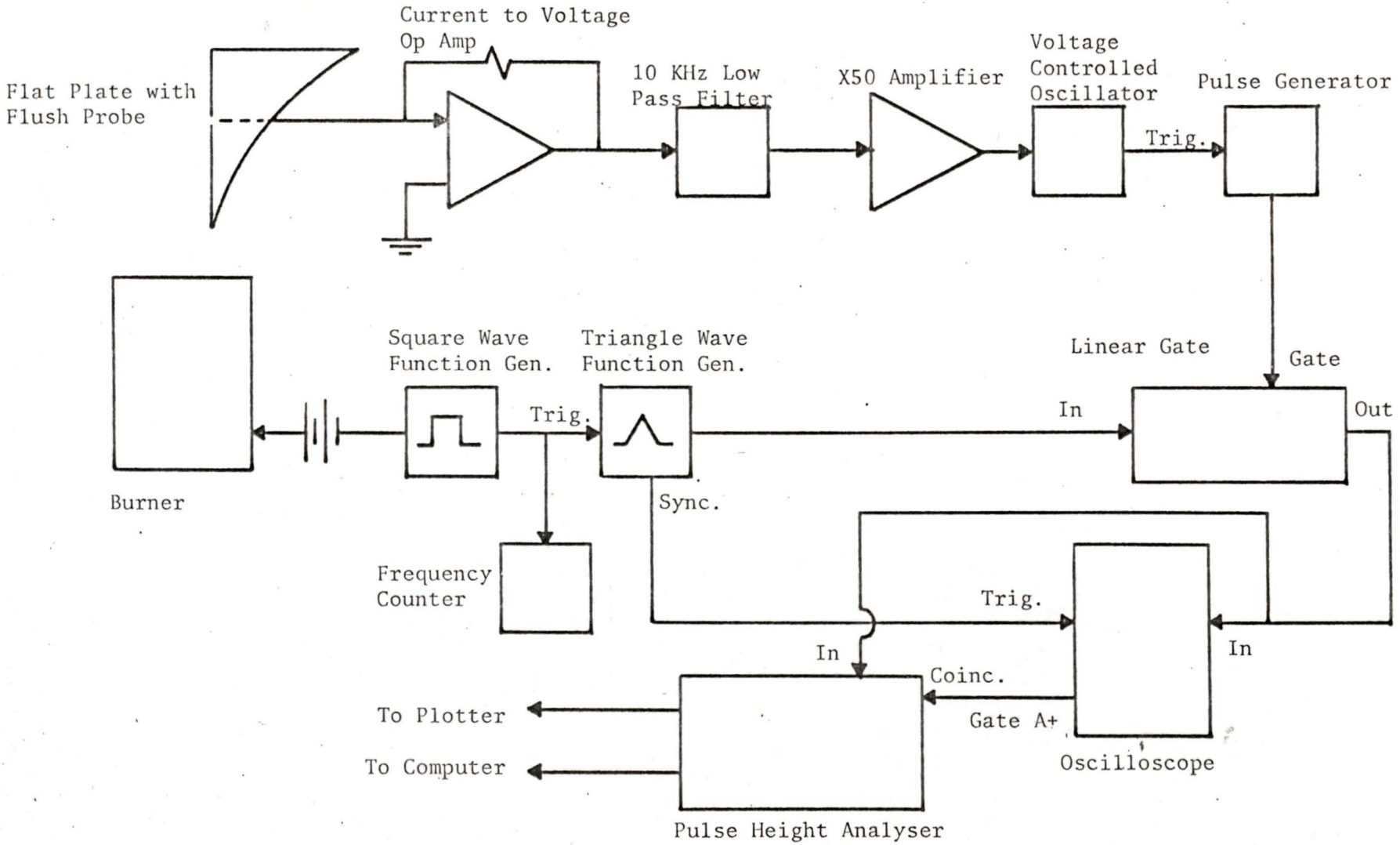

Figure 3.5. Method for Averaging the Flush Probe Signal

and flush probe current in the pulse frequency. A pulse height analyser (Northern Econ II) demodulates the signal. Briefly, the pulse height analyser (PHA), discriminates pulse height and adds one count into the one of the 512 channels of the PHA's memory which corresponds to the voltage height of the counted signal. If a train of pulses linearly increasing (or decreasing) in voltage as time progresses is fed into the PHA, the analyser's channels can be directly calibrated in time rather than voltage. Consequently, the signal going into the PHA results in counts in a channel proportional to the pulse frequency at the corresponding time. Only a portion of the signal from the linear gate is sampled by the PHA, This sampling is accomplished by using an oscilloscope (Textronix 547) in an intensified time base mode, triggered by the triangle generator. The oscilloscope gate output (Gate A^{+}) feeds into the PHA's coincidence input to gate its signal input. The PHA then adds successive gated signals to give a reconstruction of the flush probe current. Typically, the apparatus was run to sum over 2000 responses to the voltage step. By adding so many signals, unsynchronized noise added to a very small effect and the relaxation of the probe current was readily discerned. The linearity of the circuit was tested by inputting a linear ramp voltage and checking that the reconstructed signal was linear. Fig. 3.6 illustrates typical waveforms in the signal path just discussed.

Processing data accumulated on the pulse height analyser was done using a PDP 11/10 minicomputer. Data transfer to the computer was effected by modifying the teletype output of the PHA to a 600 baud rate and optically coupling this output to a video terminal port of

the computer. A program (see appendix B) was written to accept data from the PHA in character format, to convert the relavent data block into floating point numbers and then perform the data analysis. Fig. 3.7 will assist in discussing the analysis. Region A_1 is the portion of the accumulated signal where the plasma disturbance is no longer present. This region is fitted with a straight line using the method of least squares. Region B_1 is the portion of the signal where the plasma disturbance is relaxing and is approximated by a logarithmic curve (origin O is some distance away from the fitted data to avoid the singularity of the logarithm at the origin). A second approximating logarithmic curve, B_2 was fitted for a shorter channel interval further from the origin, starting where the slope of B_1 was a predetermined value. This second fit helped to avoid weighting the fitted curve with data close to the origin where information is irrelevant to the relaxation time. Retaining data close to the origin unfavourably weights the curve fit to give a relaxation time shorter than the actual time. To finally determine the relaxation time, the intersection of curves A_1 and B_2 was taken as the point where the disturbance ceased and was found using the Newton-Raphson method. Calling the channel width from the origin to the intersection of $A_1 - B_2$, τ_1 and the total signal channel width τ_2, τ_1/τ_2 is the fraction of the sampling interval that the original current spike had taken to relax.

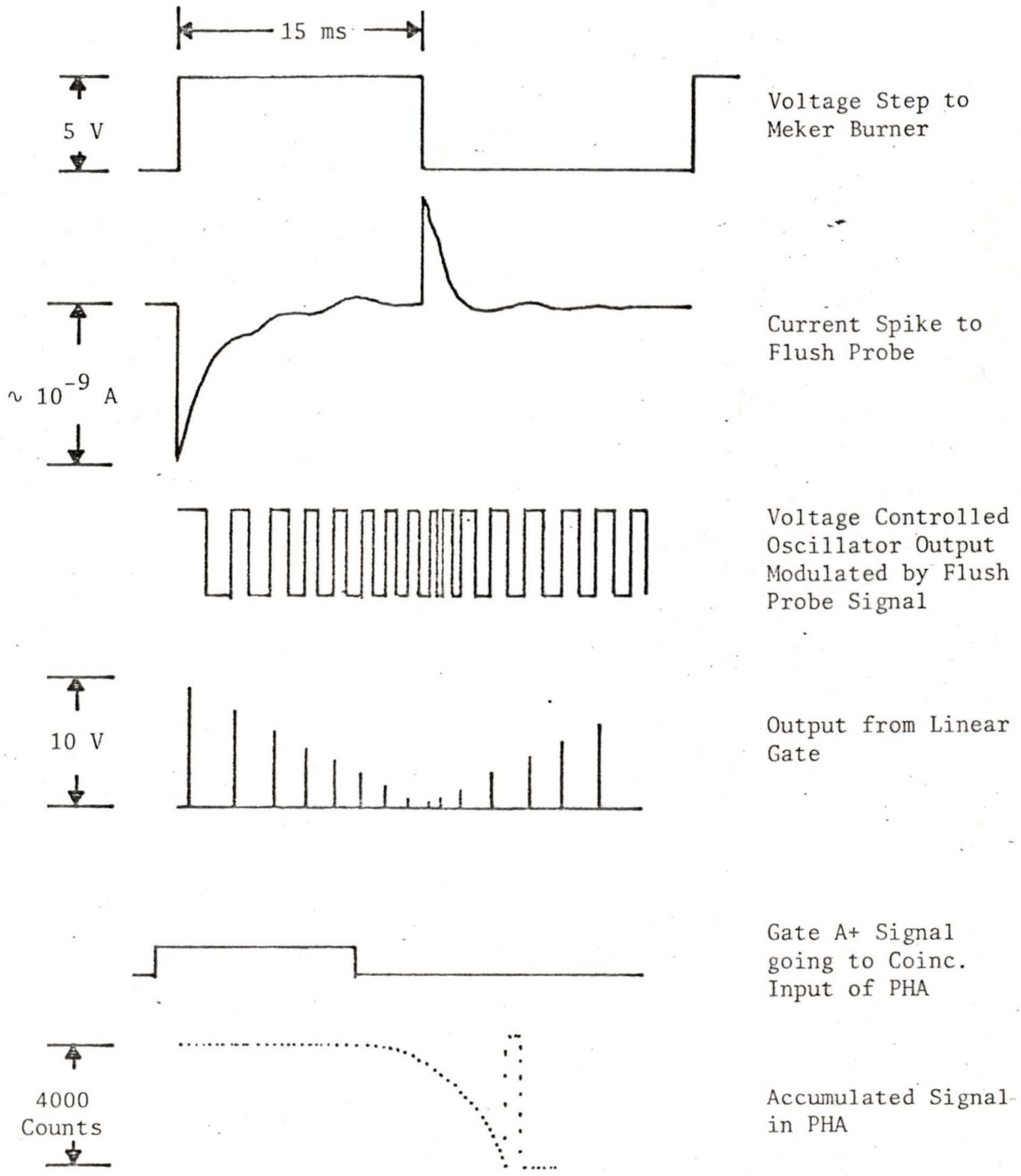

Figure 3.6. Typical Waveforms in the Averaging of the Flush Probe Currents

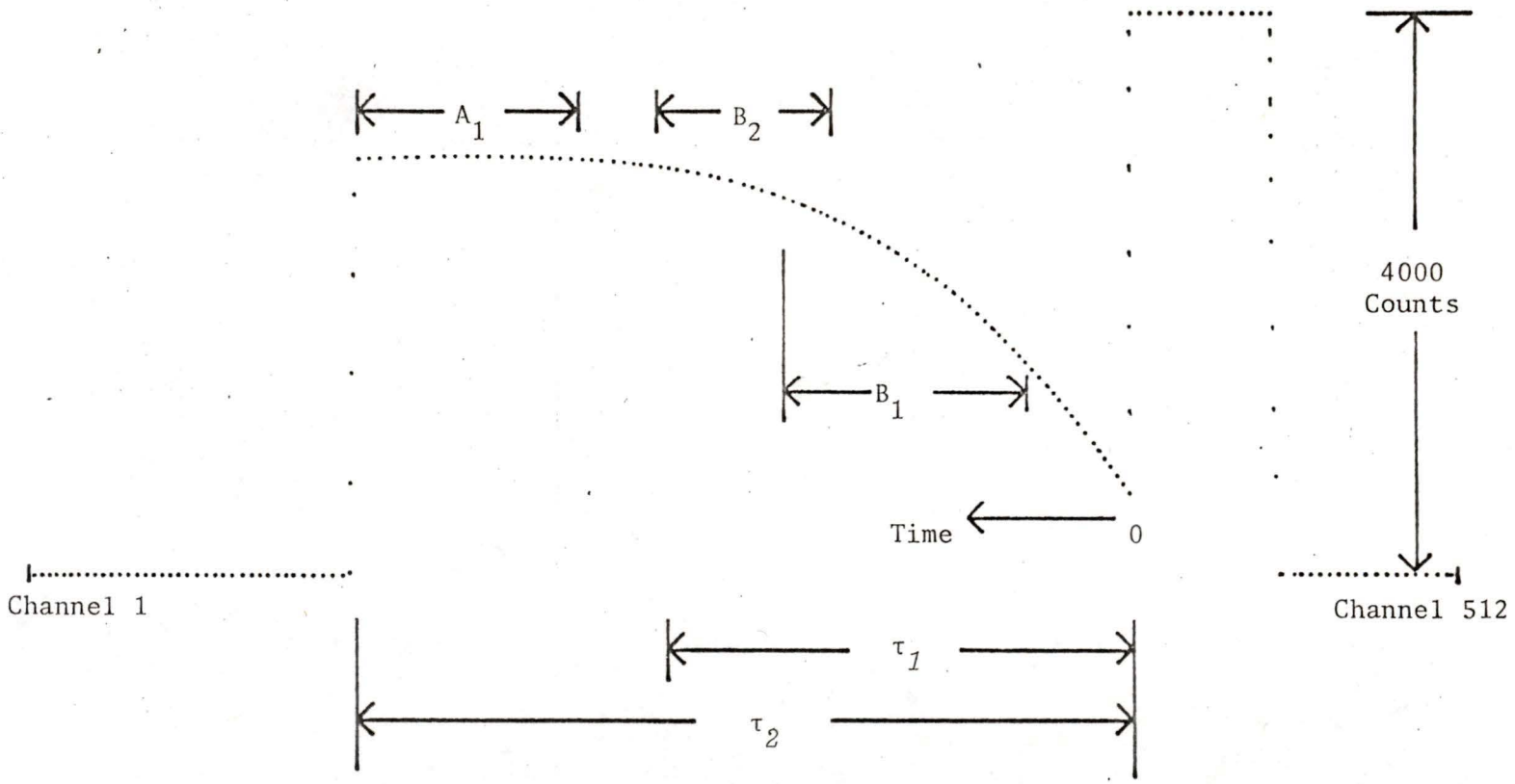

Figure 3.7. Method for Determination of Relaxation Time From the PHA Output

CHAPTER 4

RESULTS

4.1. General Discussion

Flame generated plasmas have both advantages and disadvantages in their use in experimental plasma physics. Producing these plasmas is often very simple as in this thesis where a standard laboratory Meker burner was used to generate the flame. More refined methods for creating the flames are used to give greater flow stability or some desired flame characteristic (Lawton and Weignberg, 1969). The direction of these refinements is primarily to compensate for the problems inherent in flame plasmas. Constant flame speed and ion concentration are the most severe limitations with flame plasmas with many measurements being very sensitive to them (Clements et al., 1972). Flame size can also limit the usefulness of the plasma as it becomes increasingly more difficult to control the plasma parameters as the test configuration increases in size (Lawton and Weinberg,1969).

In the experimentation for this thesis, measurements within a factor of 2 of the theoretical prediction are reasonable. Such errors are commonly experienced among researchers who have been involved with flame plasmas (Clements et al., 1972; Smy, 1976). Low probe ion currents of $O(10^{-9}$ A) were measured in this thesis and it was not uncommon for 50% fluctuations in the ion current to occur. If the plasma parameters drifted through the course of the experiment, even

larger variations occured. Signal averaging was necessary in some parts of the work to ensure that the measurements could be extracted. The methods employed in the signal averaging are outlined in the experimental section of this thesis.

4.2. Plasma Conditions

A dichotomy in the experiment came from the use of two plasma regimes. A low ion density plasma was first studied to demonstrate the feasibility of using a flat plate, generating an ion sheath around it and measuring ion current relaxation times with flush probes. The high ion density flame was used to make certain the ion sheath edge was inside the viscous and thermal boundary layers adjacent to the plate. Essential parameters for the high and low ion density plasmas are tabulated in Table 4.1. $\mathcal{X}$ and $\mathcal{Y}$ subscripts in Table 4.1 indicate quantities that were calculated with l as a scale length and $\delta(X)$ as a scale length respectively. The reason for this distinction is that one transport mechanism may dominate in the direction parallel to the plate conductor while another mechanism may control the ion transport perpendicular to the flat plate. The most relevant figures are the dimensionless quantities R_e , $R_e\alpha^2$ and $R_e\alpha^2\chi^2$. The Electric Reynolds number R_e , characterizing $\frac{\text{Ion Convection}}{\text{Ion Diffusion}}$, certainly demonstrates that ion convection will be the most important method of transporting the ions to the quasineutral region whereafter diffusion and mobility continue in transporting the ions to the probe surface. $R_e\alpha^2\chi^2$ values indicate that mobility and diffusion at the

Table 4.1. Plasma Parameters

	Low Ion Density	High Ion Density
$\tilde{D}_{+o}$	2.6×10^{-4} m^2 s^{-1}	1.3×10^{-4} m^2 s^{-1}
U_o	5 m s^{-1}	5 m s^{-1}
$\tilde{T}_o$	1500^o K	1500^o K
l	1×10^{-2} m	1×10^{-2} m
$\delta(X)$	2×10^{-3} m	2×10^{-3} m
N_o	1×10^{15} m^{-3}	1×10^{17} m^{-3}
$R_e \hat{x}$	390	770
λ_D	8.5×10^{-5} m	1.7×10^{-6} m
α	9×10^{-3}	9×10^{-4}
$R_e\alpha^2 \hat{x}$	.03	6×10^{-4}
$R_e\alpha^2\chi^2 \hat{x}$	$1.89 \cdot V^2$	$.037 \cdot V^2$
$R_e \hat{y}$	40	80
$R_e\alpha^2 \hat{y}$	.15	3×10^{-3}
$R_e\alpha^2\chi^2 \hat{y}$	$10 \cdot V^2$	$.2 \cdot V^2$

ion sheath edge may be of similar magnitude for $V = O(1)$. In both the low and high ion density plasma, the ion streamline close to the probe will be perpendicular to its surface as indicated by very low $R_e\alpha^2$ values.

4.3. D.C. Measurements of the Low Ion Density Plasma

A large sheath thickness for the low ion density plasma made it possible to measure the ion density near the flat plate probe using a rotating cylindrical probe. The results of measuring the ion densities are given in Fig. 4.1. These graphs demonstrate the voltage dependence of the ion density gradients in directions both parallel and perpendicular to the flat plate. The estimated ion current resulting from these gradients is $\tilde{D}_{\alpha o}(\Delta N/\Delta X)$. In Table 4.2 $\tilde{D}_{\alpha o}(\Delta N/\Delta X)$ is compared to the ion convection, $N_o eU_o$ in the $\hat{x}$ direction and for the diffusion in the $\hat{y}$ direction, $\tilde{D}_{\alpha o}(\Delta N/\Delta Y)$ is compared with ion flux in the simple sheath convection model (Eq. (2.2.3)).

For comparison, $R_e\,\hat{x}$ was approximately 390 (Table 4.1) while j_T/j_D in the $\hat{x}$ direction is estimated as being approximately 210 (Table 4.2). j_T is the theoretical current density which in the $\hat{x}$ direction is $N_o eU_o$. j_D is the diffusion current $\tilde{D}_{\alpha o}(\Delta N/\Delta X)$. This is an experimental verification of the ion transport conditions around the probe. $j_T/j_D \sim 4$ in the $\hat{y}$ direction which is a factor of 10 below the estimated $R_e\,\hat{y}$. The explanation is that the Electric Reynolds number in Table 4.1 was calculated by comparing the diffusion flux to the bulk ion convection flux $N_o eU_o$ rather than the ion

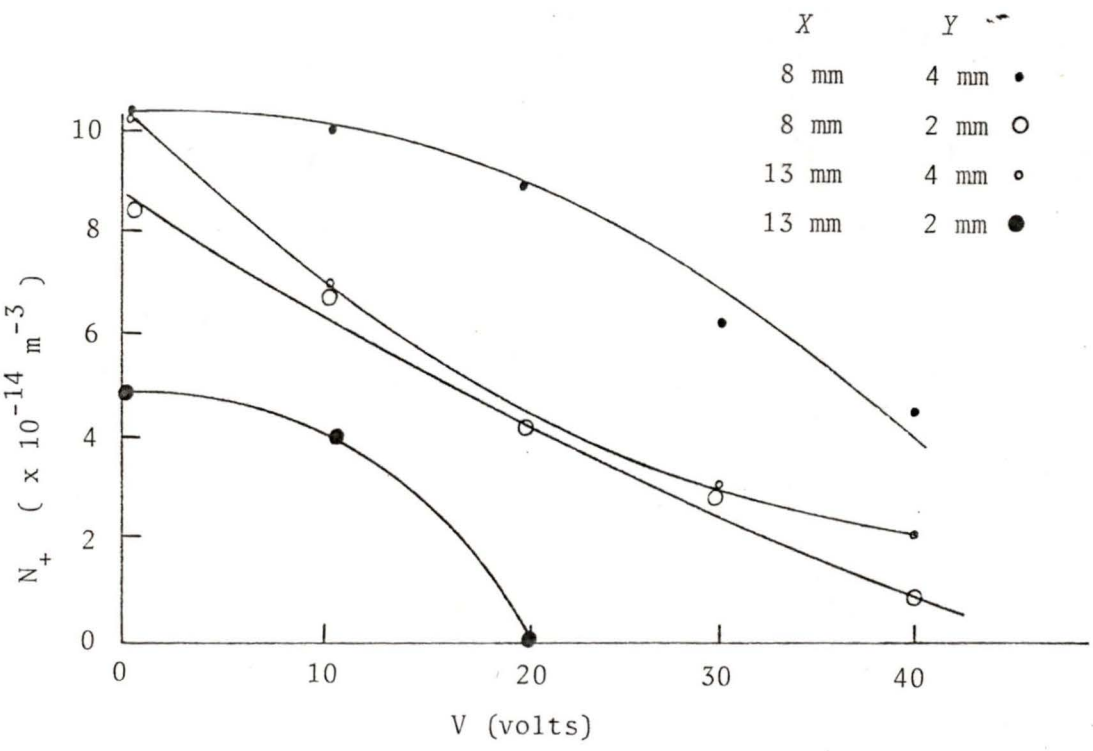

Figure 4.1. Ion Density Around the Flat Plate

(Solid lines indicate least squares fit to data)

Table 4.2. Comparison of Diffusion Currents to Convection Currents

	Current in $\hat{y}$ Direction.		Current in $\hat{x}$ Direction.	
V	X = 8 mm	X = 13 mm	Y = 2 mm	Y = 4 mm
0 V				
j_D (A m^{-2})	1.3×10^{-5}	2.2×10^{-5}	5.4×10^{-6}	1.8×10^{-6}
j_T (A m^{-2})	----------	----------	8×10^{-4}	8×10^{-4}
j_T/j_D	----------	----------	148	435
10 V				
j_D (A m^{-2})	1.5×10^{-5}	1.8×10^{-5}	5.6×10^{-6}	4.2×10^{-6}
j_T (A m^{-2})	7.5×10^{-5}	5.2×10^{-5}	8×10^{-4}	8×10^{-4}
j_T/j_D	5	2.8	143	190
20 V				
j_D (A m^{-2})	1.5×10^{-5}	1.4×10^{-5}	4.6×10^{-6}	5.0×10^{-6}
j_T (A m^{-2})	1.1×10^{-4}	7.4×10^{-5}	8×10^{-4}	8×10^{-4}
j_T/j_D	7.3	5.3	174	160
30 V				
j_D (A m^{-2})	1.4×10^{-5}	1.0×10^{-5}	3.4×10^{-5}	5.2×10^{-5}
j_T (A m^{-2})	1.3×10^{-4}	9×10^{-5}	8×10^{-4}	8×10^{-4}
j_T/j_D	9.3	9	235	155
40 V				
j_D (A m^{-2})	1.3×10^{-5}	7.0×10^{-6}	2.6×10^{-6}	4.8×10^{-6}
j_T (A m^{-2})	1.5×10^{-4}	1×10^{-4}	8×10^{-4}	8×10^{-4}
j_T/j_D	11.9	14.3	307	165

sheath convection flux which decreases $N_o eU_o$ by the factor $\partial Y_s/\partial X$. The conclusion for the low ion density plasma is that diffusion can be neglected in ion transport models and in fact this was done for the model describing the motion of the ion sheath edge in a step voltage response.

Further characterizing of the steady state ion sheath conditions around the flat plate was done using the change in the net electron current to an air cooled spherical probe to measure the ion sheath edge position as a function of plate voltage and distance from the leading edge. Fig. 4.2 summarizes the results of the measurements and compares them with the simple model of Clements and Smy (1970) and DeBoer (1968) (see Eq. (2.3.5)).

The discrepancy between the theoretical and experimental ion sheath edge position in Fig. 4.2 is explained by the ion density gradients existing in the plasma (c.f. Fig. 4.1) which cause the ion sheath thickness to increase faster than $X^{\frac{1}{4}}$ for a uniform plasma. The ion density decreased further downstream from the flat plate's leading edge and the sheath thickness increased because of the $N_o^{-\frac{1}{4}}$ dependence in Y_s . The large spherical probe size was far from an ideal test probe and limited the resolution of the measurements of the ion sheath edge position. Particularly, close to the flat plate leading edge, the sheath thickness was comparable to the test probe radius and was not expected to give very accurate measurements.

A final d.c. measurement made for the low ion density plasma experiment was done to compare the flush probe characteristics with the behaviour predicted by the sheath convection model ($j_{\tilde{t}=0^-}$ from

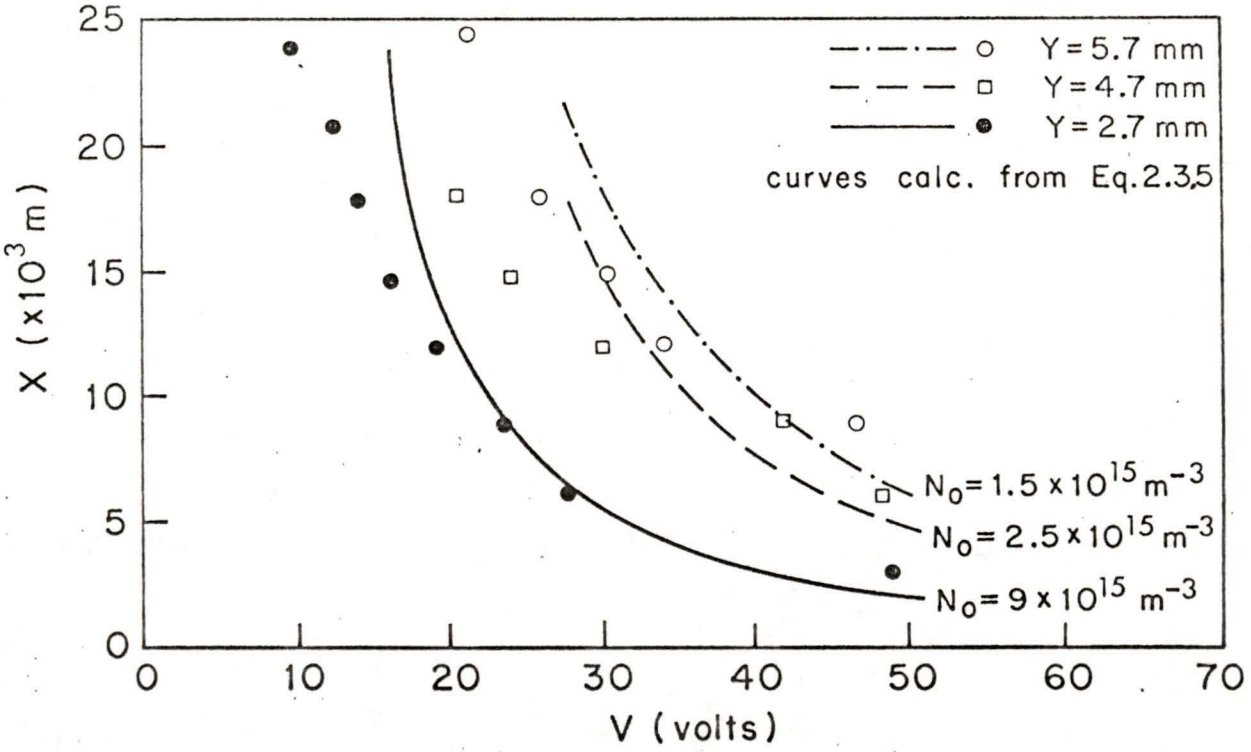

Figure 4.2. Ion Sheath Edge Position as a Function of Plate Voltage

Eq. (2.3.15)). Fig. 4.3 displays the results and the approximating sheath convection model prediction. Qualitatively, the decreasing ion density furhter upstream from the flat plate leading edge is manifested by the ion current density decreasing faster than the $X^{-3/4}$ from the simple model and is supported by the rotating probe results in Fig. 4.1 and Table 4.2. The calculated diffusion current $\tilde{D}_{\alpha o}(\Delta N/\Delta X)$ between the flush probes 1 cm and 2 cm downstream is 5.2×10^{-6} A m^{-2} which is within a factor of two of the rotating probe results. In conclusion, the results of the d.c. measurements show a significant ion gradient in the direction of the plasma flow for the low ion density flame, but the sheath convection model of plasma sheath formation holds locally along the flat plate surface. The plasma properties and flat plate probe characteristics are acceptable for using the relaxation model of section 2.3 to study the flat plate response to a negative going voltage step in the plate's bias.

4.4. Pulsed Probe in the Low Ion Density Plasma

Using the stationary spherical probe in the ion collecting mode, the sheath relaxation time to a voltage step in the plate's bias was measured. All the relaxation times were measured for an increasing negative step voltage to move the sheath to an equilibrium position further from the flat plate. Fig. 4.4 plots the results of relaxation time τ as a function of distance downstream from the leading edge. The reciprocal of the graph's slope equals the disturbance's propagation speed. From the theory for the low ion density plasma, this

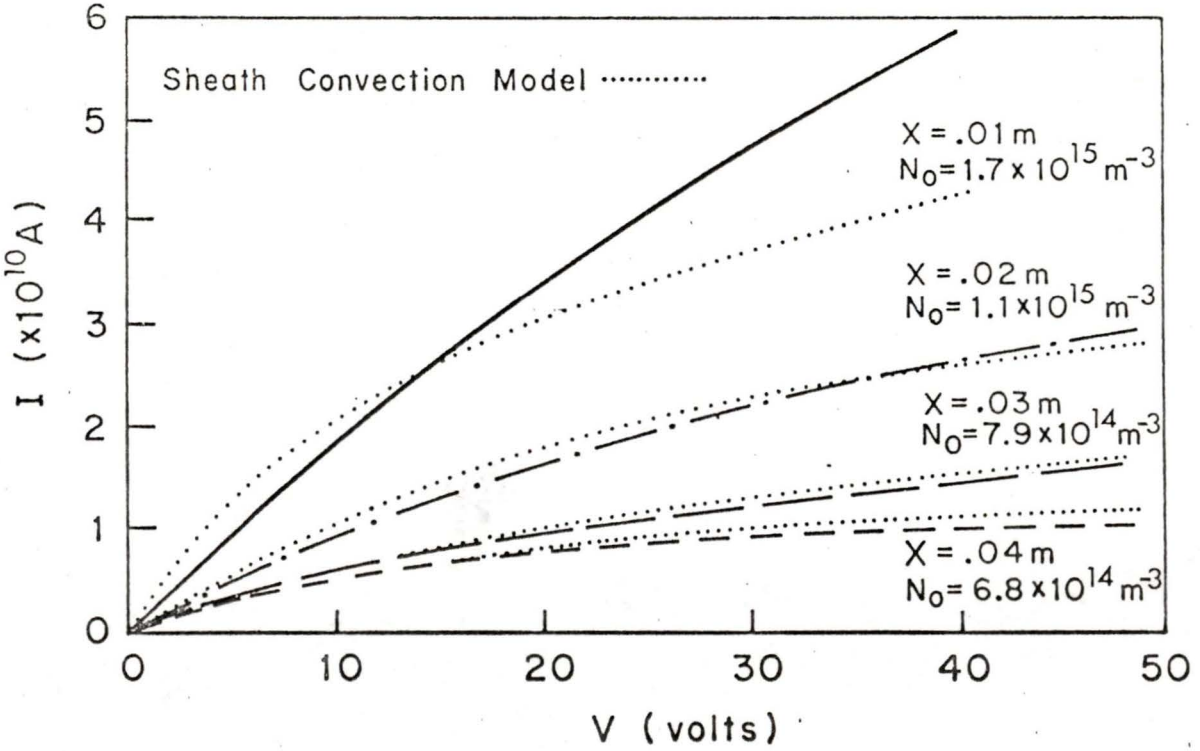

Figure 4.3. D.c. Flush Probe Characteristics in a Low Ion Density Plasma

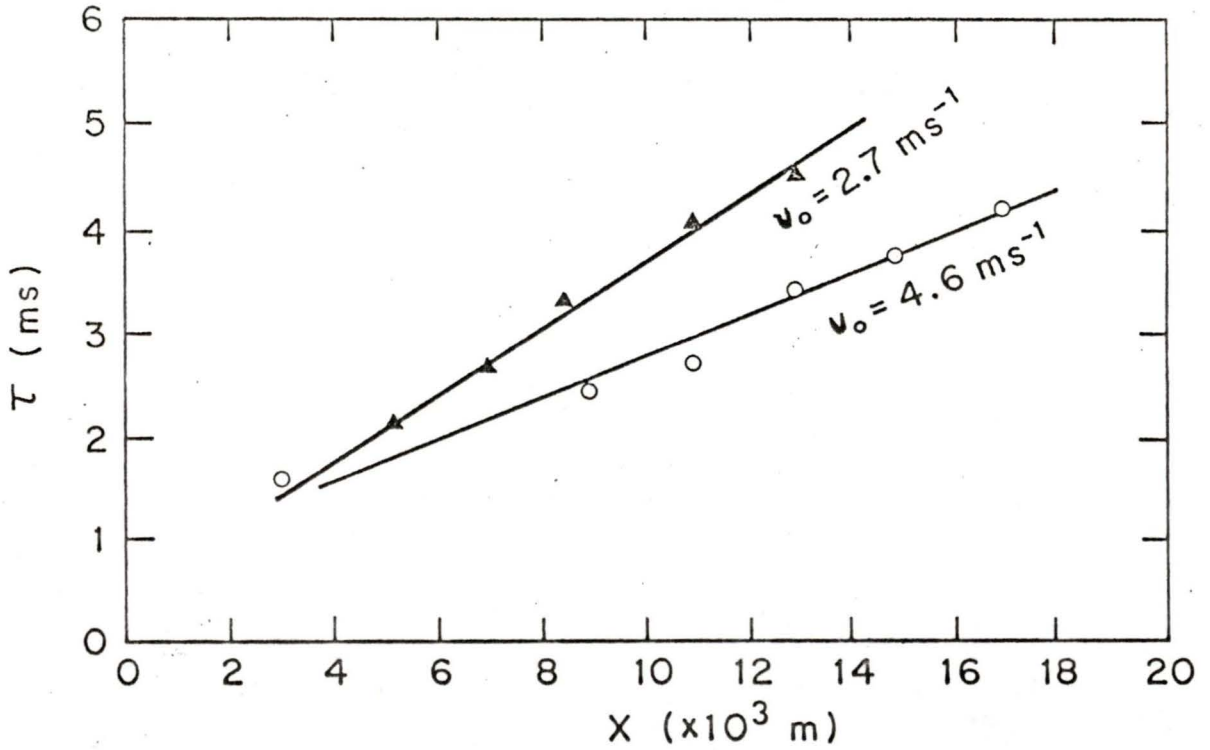

Figure 4.4. Ion Sheath Relaxation Time

is equal to the freestream plasma velocity. Two different air-propane flow rates were experimented with and gave flow speeds of 2.7 m s^{-1} and 4.6 m s^{-1} . The gas flow setting was left at the higher flow speed setting through the rest of the experimentation for both high and low density plasmas. The 4.6 m s^{-1} is 20% higher than the calculated flow speed of 3.8 m s^{-1} from the stoichiometric calculations in section 3.2. Similar results are calculated for the lower gas flow speed. A plausible explanation of this effect is that entrainment of surrounding air into the flame increased the total mass flow in the flame and gas buoyancy together gave a higher flow speed (Clements et al., 1972).

Further verification of the pulsed probe measurements was done by measuring the pulsed probe h_1/h_2 values and comparing to those calculated from Eq. (2.3.21). Table 4.3 summarizes the results from measuring the total current to the flat plate. Flush probes measured the current density at different points downstream on the flat plate and also gave h_1/h_2 values and relaxation times. The flush probe measurements displayed a greater scatter of h_1/h_2 values than did the total plate current measurements and is probably explained by realizing that a very low ion current was being detected ($\sim 10^{-9}$ A) and significant fluctuations in the current did occur because of the difficulties in maintaining a spatially and temporally uniform plasma. The σ' values were observed to correspond closely to the experimental h_1/h_2 values for the whole plate even for large voltage changes during the voltage step. The value of these results is that they encourage the possibility of using the current spike to study the viscous boundary layer when the ion density is sufficiently high to move the ion sheath

Table 4.3. Comparison of h_1/h_2 to σ and σ' Values for a Flat Plate Probe

X	V_i	V_f	h_1	h_2	h_1/h_2	σ	σ'	τ
(a) Total Probe Current								
2 cm*	-19 V	-21 V	---	---	2.2	4.3	1.5	---
2	-38	-42	---	---	2.7	4.3	1.5	---
2	-18	-22	---	---	2.3	4.7	2.3	---
2	-36	-44	---	---	2.4	4.7	2.3	---
2	-32.5	-47.5	---	---	2.7	5.4	3.1	---
2	-10	-30	---	---	6.3	10.9	6.0	---
(b) Flush Probe Current								
1 cm	-10 V	-15 V	1.7×10^{-9} A	4.1×10^{-10} A	4.2	5.6	2.1	2 ms
2	-10	-15	.346	1.42	2.4	5.6	2.5	4 ms
3	-10	-15	.285	.813	3.5	5.6	2.7	5.8 ms

* 2 cm was chosen as a mean value of X for the whole probe.

edge close to the probe.

4.5. D.C. Probe Characteristics in a High Ion Density Plasma

After having studied the operation of the flush probes in the low density plasma, the viscous boundary layer effects for a high ion density plasma were examined as outlined in section 2.4. No attempt was made to use the rotating cylindrical probe or stationary spherical probe to detect the sheath edge since it is very close to the plate at high ion densities. Fig. 4.5 shows typical current-voltage characteristics of the flush probes and compares them with predictions from the sheath convection model and the model of section 2.5. Only fair agreement is attained between either of the two models and the measured probe current. The sheath convection model is too simple an approach when the ion sheath thickness is comparable to the hydrodynamic boundary layer thickness. Correcting the sheath convection model by decreasing the mobility constant to some lower average value would only predict less current and give a large disagreement with the measurements.

There are three explanations that together could reasonably account for the discrepancy between the measured current and that in the theory of section 2.5. Fig. 4.6 shows the temperature dependence of the floating potential calculated by changing $\tilde{T}_{-o}$ in Eq. (2.2.2). This graph suggest that if the electron temperature was higher than 1500^{o} K , as first measured for the flame using an optical pyrometer, it is possible that the floating potential could be as much as $\sim$ 1 V

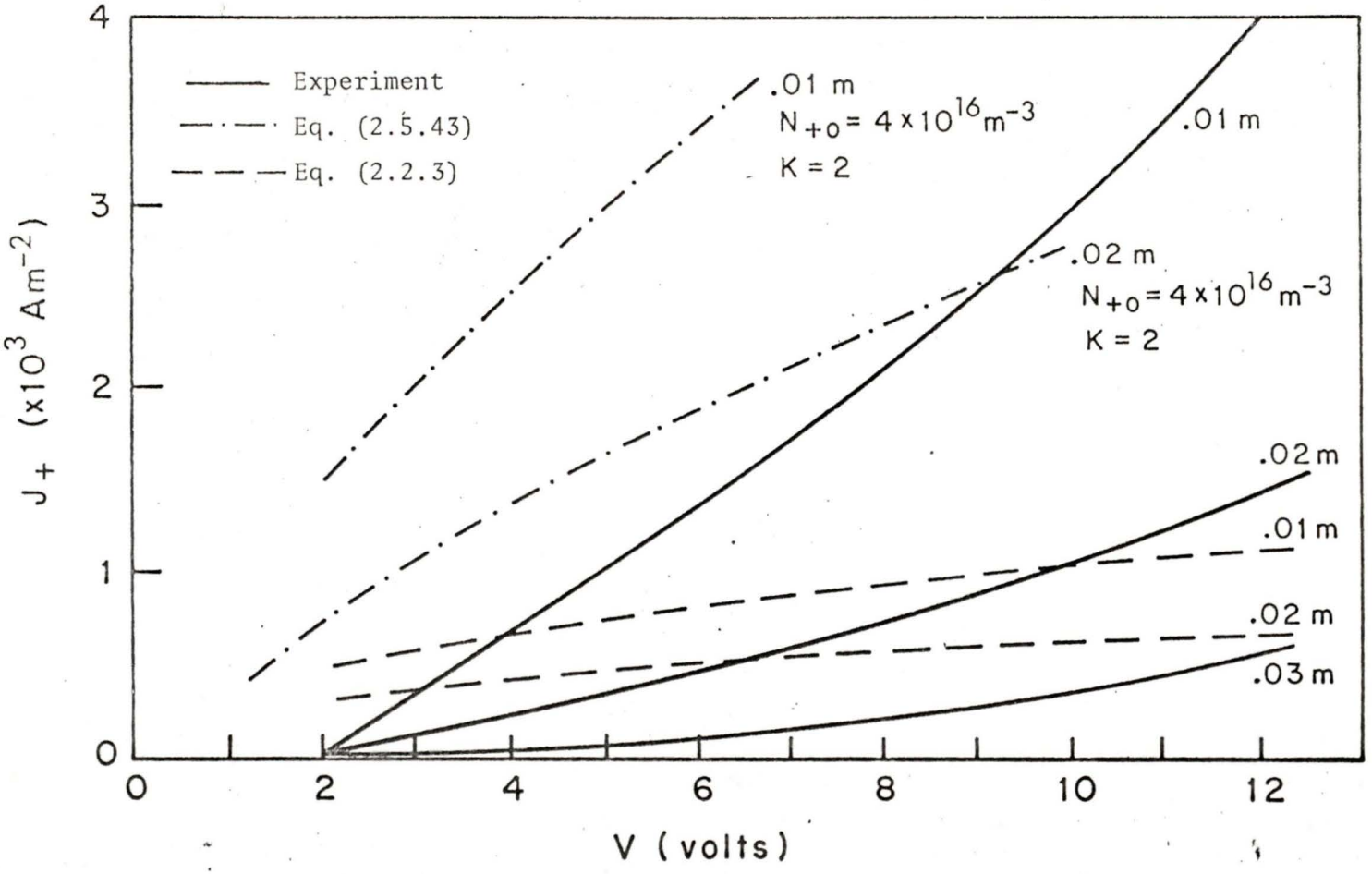

Figure 4.5. Probe Characteristics in a High Ion Density Plasma

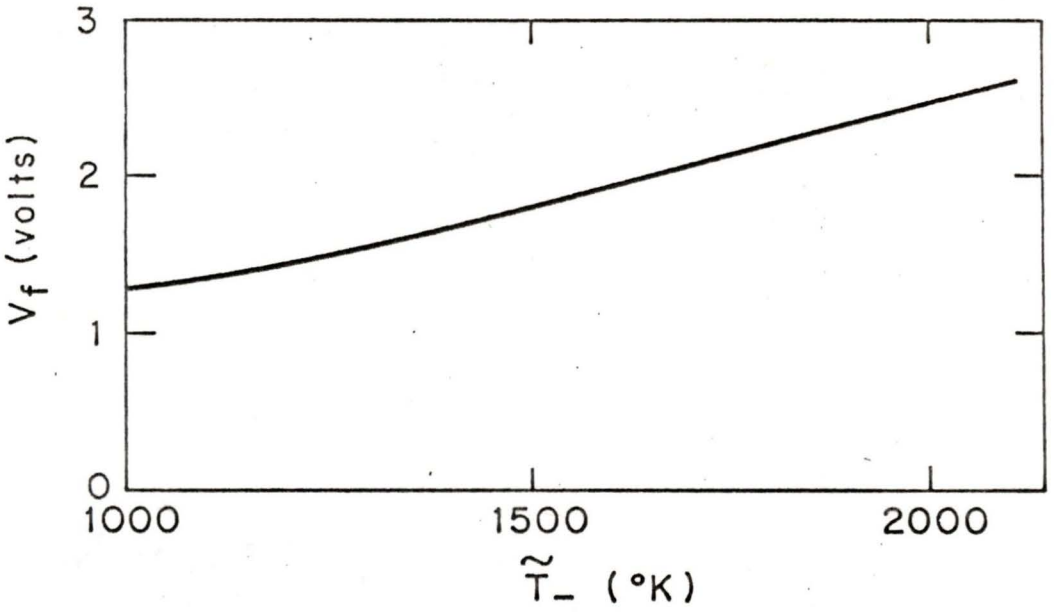

Figure 4.6. Floating Potential as a Function of Electron Temperature

higher. From the mechanism of electron generation, it is possible for the electron temperature to be higher than the flame temperature by as much as a factor of 2 (Von Engel and Cozens, 1963). A shift of 1 V will change the discrepancy from a factor of 2.5 to one of 2.3 -- not enough to account for the difference. The second explanation is from a problem inherent to the experiment. When the flame was seeded with KOH, a thin white deposit formed on the plate through the course of experimentation. Measurements with an ohmmeter immediately after turning off the flame, showed that the white film had a very high resistivity (ohmmeter reading > 10^6 ohms). With this film acting as an insulating layer, it could be expected that a significant decrease in the current density might occur. Swift and Schwar (1970) warn of this difficulty with probe contamination and the large effects it may have on the ion collecting characteristics. Clements (1975) also reported difficulties in using probes to study the ion density in an MHD combustion duct seeded with KOH. Clements observed the deposition of a white powder on his probes that interfered with his ion current measurements. From chemical analysis, Clements found that the powder was K_2CO_3 and it is probable that the deposit in this experiment was also K_2CO_3. Finally, the ion flux to the probe is typically a significant portion of the total ion flow from the burner. At an ion density of 4×10^{16} m^{-3} and for the gas flow of the experiment, the total ion flow would be 3.2×10^{-5} A . For an average ion flux to the probe of 4×10^{-3} A m^{-2} and a total collecting surface of 20 cm^2, the probe ion collection would represent 25% of the total ion flux from the flame. It is likely this has consequences on the current-voltage character-

istics and suggests that the probe ion flux could be less than predicted simply because of the large perturbation the probe had on the flame ion concentration. These three effects mentioned may have cumulatively resulted in the lower ion flux to the flush probes.

The validity of the model in this thesis in predicting ion current to the probe was checked by comparison to two simpler models which have been proposed by earlier authors. The parameter f_2 in Eq. (2.5.44) for moderate potentials (4 - 10 V) using a high ion density plasma ($\sim 10^{17}$ m^{-3}) had a range of 2×10^{-21} to 10×10^{-21}. Chung and Blankenship (1966) derived the ion saturation current for a self similar boundary layer flow with frozen chemistry as

$$j_{t,sat} = \frac{D_{+o} N_o e}{l^{\frac{1}{2}}} \left(\frac{U_o \rho_o}{\mu_o} \right) \left(\frac{\rho_w \mu_w}{\rho_o \mu_o} \right)^{.2} \left[1 + \frac{\tilde{T}_-}{\tilde{T}_+} \right] (0.207 + 0.128 (\mu_o / \rho_o \tilde{D}_{+o})) \tag{4.5.1}$$

For the plasma conditions of the experiment and modelled in the theory, Eq. (4.5.1) gives $j_{t,sat} = 6 \times 10^{-21} N_o / l^{\frac{1}{2}}$. Even with their assumption of frozen chemistry, good agreement is seen with the range of f_2 calculated in the theory. Another comparison for the model in this thesis can be made with that of Clements and Smy (1971) who used sheath convection corrected for a temperature gradient close to the plate. Their theory was done for a conductor embedded in an insulator, but the difference between this case and the model here manifests itself primarily at the plate's leading edge where the ion sheath and hydrodynamic layer thicknesses are changing rapidly. Since both models are considering current far downstream of the plate's leading edge, the comparison can be expected to be close. For the conditions of

this experiment and small potentials with the ion sheath inside the hydrodynamic layer, Clements and Smy's theory predicts $j_{t,sat} \simeq 5 \times 10^{-21} N_o/l^{\frac{1}{2}}$. One feature common to all three models is the $N_o/l^{\frac{1}{2}}$ dependence in the current density. This similarity is a substantial reinforcement of confidence in the proposed model. Neither of the two previously mentioned theories adapt to the change of current with voltage but rather, examine only the ion saturation current for the thin sheath. The advantage of this new model lies in it's ability to calculate the changing ion current as the plate voltage changes when the ion sheath is thin compared to the viscous and thermal boundary layers.

4.6. Pulsed Probe Characteristics

The most difficult part of the experiment came from merging the high ion density flush probe behaviour with the step voltage response. The KOH seeder used to generate the plasma suffered from both short period ($\sim$ 10 ms) and long period ($\sim$ 100 s) fluctuations. The short period fluctuations in the ion density and flow speed were critical because they gave noise comparable in magnitude to the measured signal $\sim 1 \times 10^{-9}$ A and a duration similar to that of the relaxing signal after the step in the probe bias. This problem necessitated the use of the averaging circuit described in section 3.3. Normalization of the averaged signal to the maximum current pulse height precluded the calibration of the current axis of the relaxation curves but the qualitative nature of the response and the relaxation time were dis-

played. Fig. 4.7 exhibits typical relaxation curves accumulated in the signal averaging instrumentation. The relaxation times indicated on the curves are those calculated from the computer analysis of the data in the pulse height analyser. Again, because of the averaging scheme, σ' values were not compared with h_1/h_2 values, but for the test conditions h_1/h_2 was 2 - 3 .

One asset of the averaging circuit in spite of the long time required to accumulate a single point and calculate the relaxation time, ($\sim$ 3 hours total time/point) was the reliability of the calculated time. Time measurement for the flush probe 0.01 m downstream of the plate's leading edge was difficult to analyse because of the small variation of the relaxation time with probe voltage. As demonstrated in Fig. 4.8 (c) by the spread of data points, further downstream of the plate's leading edge, a scatter of data points was observed. This problem may be explained by the unsteady flow of the flame gases and disturbances caused by ambient air turbulence and changing atmospheric conditions. 0.04 m downstream was found to be the limit for measuring the relaxation time. Figs. 4.8 (a) to 4.8 (c) show the relaxation time as a function of plate voltage 0.02 m, 0.03 m and 0.04 m downstream from the plate's leading edge. The measured ion density indicated for each set of experimental results is used to calculate the theoretical predictions for $K = 0$ and $K = 1$ (a measure of cooling effects on the ion sheath as outlined in section 2.5). The rotating probe measurements of the ion density are accurate to 30% (Clements et al., 1972) and could explain some of the difference between the predicted and actual voltage dependence of the relaxation

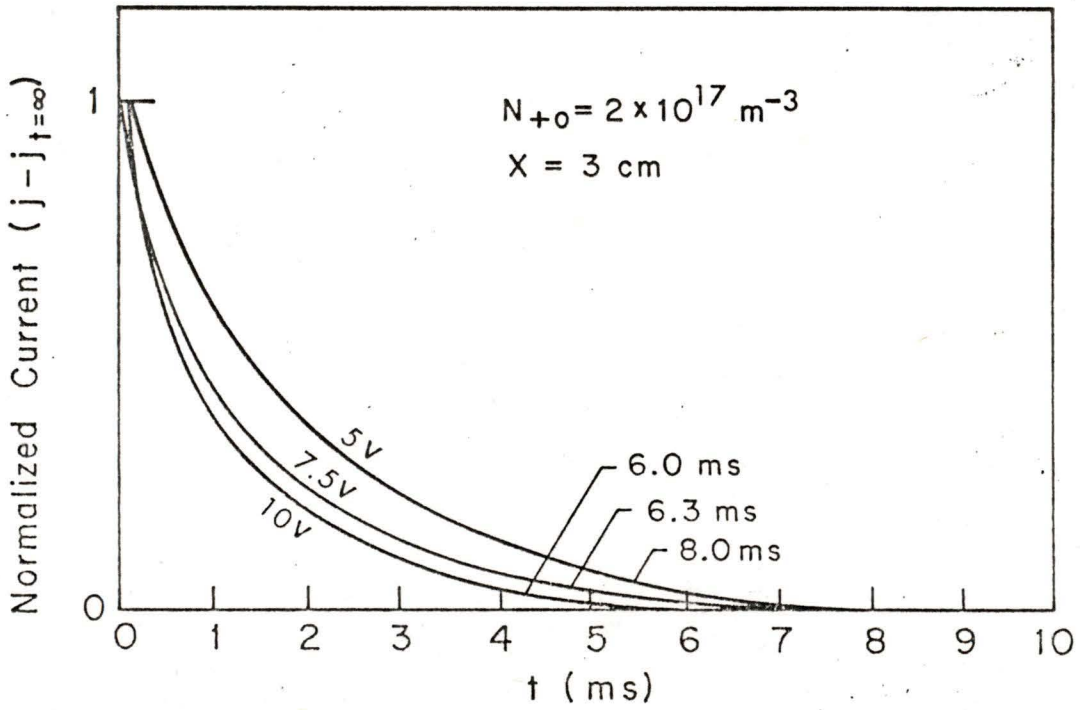

Figure 4.7. Typical Relaxation Curves

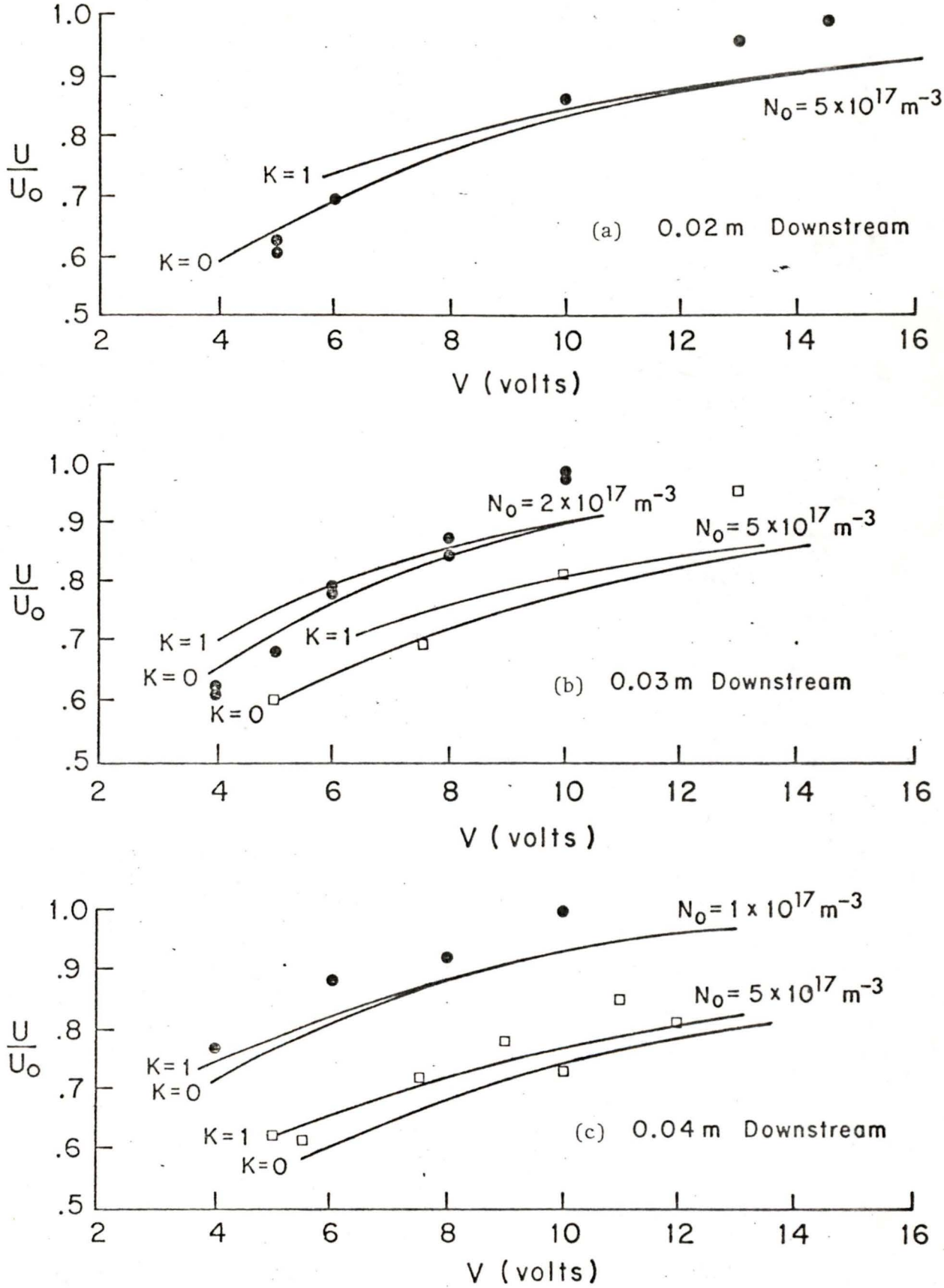

Figure 4.8. Measured Average Flow Speed as a Function of Plate Voltage. (Solid Lines from Theory)

time.

An inherent drawback of the model prediction is assuming that the step voltage disturbance travels parallel to the flat plate rather than along the ion sheath edge. This simplification was done because of the inapplicability of the theory close to the plate's front edge where the characteristic length and sheath thickness are comparable in size. The relaxation time can be expected to be longer than predicted because the sheath edge is closer to the flat plate nearer the leading edge. The sheath convection model when used to predict the relaxation time fails by nearly a factor of ½ too low through the range of ion densities and voltages in the experiment. Experimental measurements had U/U_o limited to >0.6 because at lower voltages, the electron flux became significant and because of the high electron mobility, the relaxation time decreased as the voltage was further decreased.

A direct comparison of the relaxation data to the theoretical prediction can be conveniently done by converting the flat plate voltages to the f_3 values using Eq. (2.5.45) and then calculating $\frac{U_{measured}}{U_{theory}}$. $U_{measured}$ is the speed calculated from the relaxation times in the experiment. U_{theory} is the theoretical speed that corresponds to the calculated f_3 values. Fig. 4.9 shows the results of these calculations by plotting $\frac{U_{measured}}{U_{theory}}$ as a function of f_3 (K = 0). This figure shows that the measurements fall very close to the expected values with maximum deviations of 12% from $\frac{U_{measured}}{U_{theory}} = 1$. The mean of $\frac{U_{measured}}{U_{theory}}$ is 1.02 which strongly suggests that the experiment was successful in measuring the plasma flow speeds in the viscous boundary layer adjacent to the flat plate.

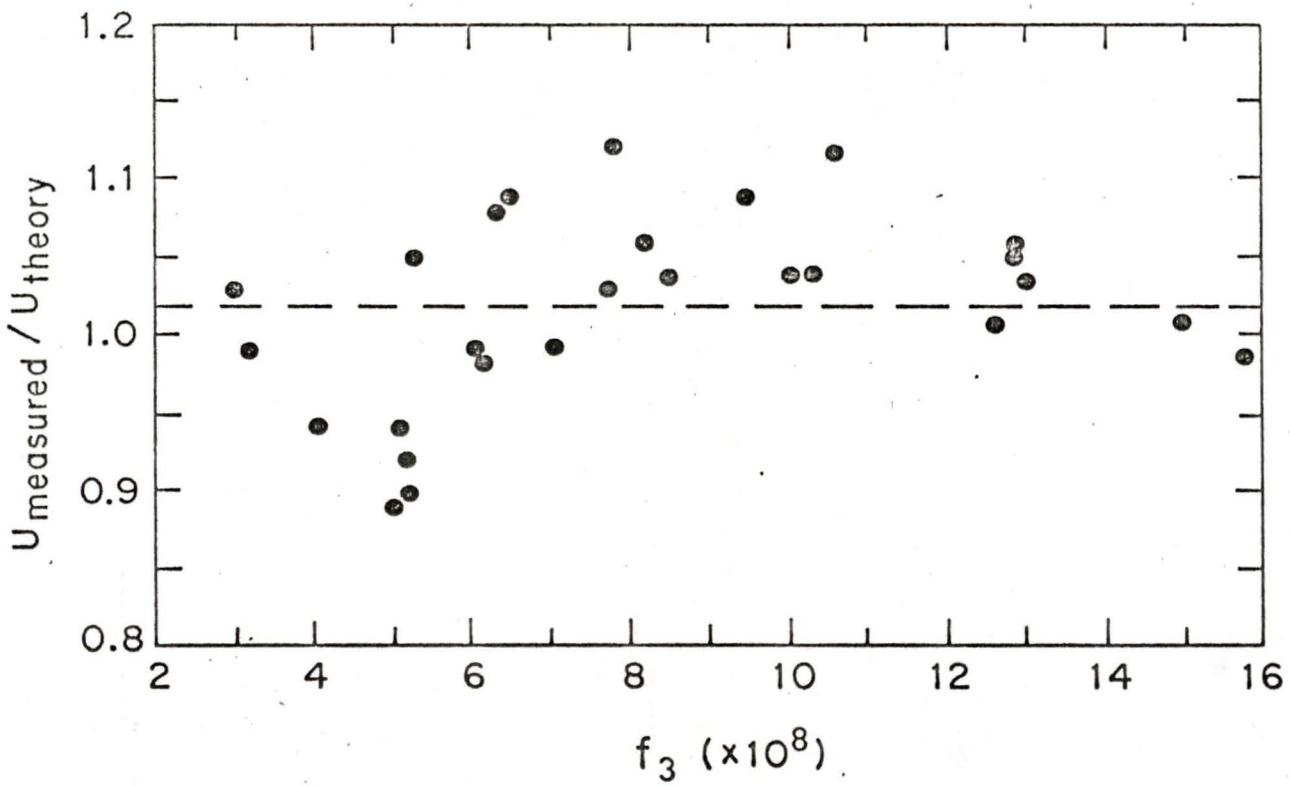

Figure 4.9. $\frac{U_{measured}}{U_{theory}}$ from Current Relaxation Measurements

CHAPTER 5

CONCLUSIONS

The operation of a flat plate probe in a continuum flowing plasma was investigated in this thesis and certain properties were experimentally ascertained. Ion transport conditions were studied and it was demonstrated that for a large Electric Reynolds number, convection dominates over diffusion in supplying ions to the ion sheath edge around the probe. D.c. flush probe characteristics were measured for both low ion density (10^{15} m^{-3}) and high ion density (10^{17} m^{-3}) plasma. Good agreement between theory and experiment was found for the low ion density plasma but at high ion density, agreement was only within a factor of 2. Such a discrepancy is not unusual in plasma measurements and difficulties in the experiment could account for the difference.

The flush probe step voltage response has been explained using a first order theory of ion collection in a low ion density plasma. A current spike was observed when the ion current overshot the equilibrium current for the new probe potential. The σ' values were on the average 25% lower than the observed h_1/h_2 , but considering the approximations in the theory and difficulties in making measurements, the agreement was good. The benefit of the current spike was that it provided a signal which was utilized to study the hydrodynamic flow properties of the plasma around the probe. By developing a theory to predict the ion sheath thickness when the ion sheath edge was inside the thermal and viscous boundary layers, it was possible to examine

the velocity profile of the viscous boundary layer. Agreement between the predicted and measured relaxation of flush probe current was within 10% which verified that the technique was feasible. Better agreement could have been sought for by refining the theory, but it is more probable that improvement of the experimental apparatus would be more worthwhile. The aspirator used to introduce the potassium hydroxide to the flame was particularly limiting in the control of both the flow speed and ion density. Noise in the flush probe current was troublesome and could be improved with better methods in generating the plasma. If improvements in the plasma production are made, it would be fruitful to do further work on the flush probe relaxation for a greater range of the plasma's ion density and flow speed. Experimenting with very high ion densities (10^{20} m^{-3}) could be particularly interesting since the ion sheath edge would be close to the probe to give long relaxation times and enhance the viscous and thermal boundary layer effects on the d.c. probe characteristics. The probe signal would also increase proportionately with the higher ion density and reduce the current noise problem.

REFERENCES

Ashton, A.F. and Hayhurst, A.N. 1973. Combust. Flame, 21, 69.

Bell, J.C., Bradley, D. and Jesch, L.F. 1971. Proc. 13th Int. Symp. on Combustion, Pittsburg, 345.

Bradley, D. and Ibrahim, S.M.A. 1974. J. Phys. D: Appl. Phys. 7, 1377.

Burke, A.F. 1968. AIAA Paper No. 68-166, 6th Aerospace Sciences Meeting, New York.

Chen, F.F. 1965. Plasma Diagnostic Techniques, ed. R.H. Huddlestone and S.L. Leonard, (Academic Press, London).

Chung, P.M. and Blankenship, V.D. 1966. AIAA, 4, 442.

Chung, P.M., Talbot, L., and Touryan, K.J. 1975. Electric Probes in Stationary and Flowing Plasmas: Theory and Application, (Springer-Verlag, New York), Chapter 3.

Clements, R.M. and Smy, P.R. 1969. J. Appl. Phys., 40, 4553.

Clements, R.M. and Smy, P.R. 1970. J. Appl. Phys., 41, 3745.

Clements, R.M. and Smy, P.R. 1970. IEEE Trans. Instr. Meas. IM-19, 167.

Clements, R.M. and Smy, P.R. 1971. IEEE, 59, 706.

Clements, R.M., MacLatchy, C.S. and Smy, P.R. 1972. J. Appl. Phys. 43, 31.

Clements, R.M. and Smy, P.R. 1974. J. Phys. D: Appl. Phys., 7, 551.

Clements, R.M. 1975. Combust. Flame, 25, 187.

Clements, R.M., Oliver, B.M. and Smy, P.R. 1977. J. Phys. D.: Appl. Phys. 10, 2213.

Cobine, J.D. 1958. Gaseous Conductors, (Dover, New York), p. 128.

DeBoer, P.C.T. 1973. AIAA, 11, 1012.

DeBoer, P.C.T. and Johnson, R.A. 1968. Phys. Fluids, 11, 909.

DeBoer, P.C.T., Johnson, R.A. and Grimwood, P.R. 1969, Proc. 7th Int. Shock Tube Symp., 795.

Dukowicz, J.K. 1969. CAL Rep. No. RA-2641-Y-1, Buffalo, New York.

Dukowicz, J.K. 1970. CAL Rep. No. AN-2755-Y-1, Buffalo, New York.

Greenspan, D. 1974. Discrete Numerical Methods in Physics and Engineering, (Academic Press, New York).

Johnson, R.A. and DeBoer, P.C.T. 1973. AIAA, 10, 664.

Krall, N.A. and Trivelpiece, A.W. 1973. Principles of Plasma Physics, (McGraw-Hill, New York).

Lam, S.H. 1964. AIAA, 2, 256.

Langmuir, I. 1924. Phys. Rev. 33, 954.

Langmuir, I. and Mott-Smith, H.M. 1926. Phys. Rev. 28, 727.

Lawton, J. and Weinberg, F.J. 1969. Electrical Aspects of Combustion, (Clarendon Press, Oxford).

Loeb, L.B. 1961. Basic Processes of Gaseous Electronics, (University of California Press, Berkeley), p. 40.

Maclatchy, C.S., Budgel, P.C. and Miner, J.R. 1974. Can. J. Phys. 52, 1057.

Miller, W.J. 1973. Proc. 14th Int. Symp. on Combustion, Pittsburg, 307.

Noor, A.I., Smy, P.R. and Clements, R.M. 1977. J. Phys. D: Appl. Phys. 10, 1643.

Nasser, E. 1971. Fundamentals of Gaseous Ionization and Plasma Electronics, (Wiley Interscience, New York), p. 188.

Oliver, B.M. and Clements, R.M. 1975. J. Phys. D: Appl. Phys. 8, 914.

Polhausen, K. 1921. ZAMM, 1, 252.

Rosa, R. 1971. J. Phys. A: Gen. Phys. 4, 934.

Russo, A.J. and Touryan, K.J. 1972. AIAA, 10, 1675.

Sandhu, S.S. and Weinberg, F.J. 1975. Comb. and Flame, 25, 321.

Schlichting, H. 1968. Boundary Layer Theory 6th ed. translated Kestin, J. (McGraw-Hill, New York).

Self, S.A. and Kruger, C.H. 1977. Journal of Energy, 1, 25.

Smy, P.R. 1976. Advances in Physics, 25, 517.

Smy, P.R. and Noor, A.I. 1976. J. Appl. Phys. 47, 1327.

Sonin, A.A. 1967. J. Geophys. Res. 72, 4547.

Stahl, N. and Su. C.H. 1971. Phys. Fluids, 14, 1366.

Stewartson, K. 1964. The Theory of Laminar Boundary Layers in Compressible Fluids, (Clarendon Press, Oxford), p. 25.

Su, C.H. 1965. AIAA, 3, 842.

Su, C.H. and Lam, S.H. 1963. Phys. Fluids, 6, 1479.

Swift, J.D. and Schwar, M.J.R. 1970. Electric Probes for Plasma Diagnostics, (Iliffe Books Ltd., London), p. 251.

Thomas, D.L. 1969. Electron. Lett. 5, 341.

Von Engel, A. and Cozens, J.R. 1963. Proc. Phys. Soc. 82, 85.

APPENDIX A

PROGRAM FOR EVALUATING f_1, f_2 AND f_3 OF SECTION 2.5.

The annotations in the program are self explanatory and identify different sections of the calculations. The data created is outputted into a file designated LPOUT.T@ but a program modification can have the data outputted to the user's terminal. Typically, the program takes about 1 minute to generate a single data point or 30 minutes for a complete set of data for given input parameters. The input parameters for the program are V2 , B , C and D+ . These variables are identified in the symbol table below. In particular, B = $1/\beta$ with β from Eq. (2.5.20) and α in β (Eq. (2.4.12)) was calculated using Simpson's Rule on a calculator. C was evaluated from Eq.(2.5.32) at $\gamma = 1/\beta$ by the same method as α . Following the program listing, a typical output for a given set of input parameters is given.

Important Variables in the Program

B = $1/\beta$ (Eq. (2.5.20))

C $n'(1/\beta) = C(1 - n)$ (Eq. (2.5.32))

D1 = Freestream Ambipolar Diffusion Coefficient

H = Step width of γ in Runge Kutta Solution of Eq. (2.5.34)

I3 = Double Integral Eq. (2.5.41)

K = Measure of Plasma Nonequilibrium (Eq. (2.5.33))

N = $n(1/\beta)$

N1 = $n'(1/\beta)$

U = $U_{average}/U_o$ (Eq. (2.6.2))

V1 = n' at sheath edge

V2 = $\tilde{T}_w/\tilde{T}_o$

W = $\tilde{T}/\tilde{T}_o$

X1 = γ_{sheath}

```
1 REM-PROGRAM FOR CALCULATING I-V CHARACTERISTICS OF FLUSH PROBES
2 H=-.02 \ PRINT 'INPUT V2,B,C,D+' \ INPUT V2,B,C,D1
3 OPEN 'LPOUT.T@' FOR OUTPUT AS FILE #1, FILESIZE 200 \ S2=2 \ K2=1 \ K=-1
4 PRINT #1,'V2=';V2;'B=';B;'C=';C;'D+=';D1 \ PRINT #1,' '
5 PRINT #1,"K          N(1/B)        N'(1/B)          N'(S)          G(S)          F1
6 REM-
7 REM- LINES 11 TO 100 SOLVE FOR ION SHEATH EDGE USING RUNGE-KUTTA
8 REM- METHOD FOR EQUATION 2.5.34
9 REM-
10 FOR J=1 TO 3 \ K=K+K2
11 FOR L=80 TO 99
12 REM- L MAY NEED TO BE CHANGED FOR DIFFERENT INPUTTED PARAMETERS
14 N=L/100 \ N1=C*(1-N)
15 X1=B \ Y1=N \ V1=N1
16 PRINT "*";
20 X=X1 \ Y=Y1 \ V=V1
25 GOSUB 1000
30 M0=H*F
35 X=X+H*.5 \ Y=Y+V*H/2 \ V=V+M0/2
40 GOSUB 1000
45 M1=H*F
50 Y=Y+M0*H/4 \ V=V-H0/2+M1/2
55 GOSUB 1000
60 M2=H*F
65 X=X+H*.5 \ Y=Y1+V1*H+M1*H/2 \ V=V1+M2
70 GOSUB 1000
75 M3=H*F
80 Y1=Y1+H*V1+H*(M0+M1+M2)/6
90 V1=V1+(M0+2*M1+2*M2+M3)/6
95 X1=X1+H
98 IF X1<0 GO TO 200
100 IF Y1>0 GO TO 20
101 REM-
102 REM-LINES 110 TO 118 CALCULATE F1,F2,F3 OF EQUATIONS 2.5.43,
104 REM- 2.5.44, 2.5.45
105 REM-
110 F2=V1*W↑2*1.60200E-19*(2.5*D1)↑.5
111 GOSUB 1590
112 F3=3.07000E-05*(6*V1*D1/2)↑.5*I3*W
113 F1=X1*(D1/5)↑.5
114 DEF FNU(R,S)=4*R*S↑.5+4*R↑3/S↑.5-R↑4/S
115 A=X1/B \ X0=A↑2 \ D=FNU(A,1) \ U=D-FNU(A,X0)+X0
117 PRINT 'N(1/B)=';N;'G(S)=';U;'VOLT.=';F3
118 PRINT #1,K,N,N1,V1,U,F1,F2,F3
120 NEXT L
121 PRINT #1,"-----------------------------------------"
122 NEXT J
123 GOSUB 1500
125 GO TO 2000
200 PRINT #1,"SLN NOT POSSIBLE AT N=",N
205 GO TO 122
206 REM-
207 REM-LINES 1000 TO 1020 CALCULATE RIGHT HAND SIDE OF EQUATION 2.5.34
208 REM-
```

```
1000 G=2*(X/B)-2*(X/B)↑3+(X/B)↑4
1005 G1=2/B-6*(X/B)↑2/B+4*(X/B)↑3/B
1015 W=V2+(1-V2)*G
1017 T=(2*W*(1-V2)*G1+X*G/2)*V
1018 IF 1/W>2 GO TO 1019 \ D9=K*((Y/W)↑2-W↑.5*EXP(33.6*(1-1/W))) \ GO TO 1020
1019 D9=K*(Y/W)↑2
1020 F=-(T-D9+X*Y*G1/2)/W↑2
1025 RETURN
1500 IF S2=5 GO TO 1520
1505 S2=5 \ GO TO 1525
1520 S2=2
1525 RETURN
1530 REM-
1531 REM- LINES 1590 TO 1790 CALCULATE DOUBLE INTEGRAL OF EQUATION 2.5.41
1532 REM-
1590 E0=21 \ E2=X1/B/10 \ M1=1 \ S4=0
1610 FOR E1=0 TO 9
1620 E0=E0-2 \ E3=(X1/B-E1*E2)/(E0+1)
1630 S6=0 \ M2=1
1640 FOR E4=0 TO E0
1650 E5=E1*E2+E3*E4
1660 S6=S6+M2/(V2+(1-V2)*(2*E5-2*E5↑3+E5↑4))
1670 IF M2=1 GO TO 1690 \ IF M2=2 GO TO 1690 \ M2=2 \ GO TO 1700
1690 M2=4
1700 NEXT E4
1710 S6=S6+1/(V2+(1-V2)*(2*X1/B-2*(X1/B)↑3+(X1/B)↑4))
1720 I4=SQR(S6*E3/3)
1730 S4=S4+M1*I4 \ IF M1=1 GO TO 1760 \ IF M1=2 GO TO 1760 \ M1=2 \ GO TO 1770
1760 M1=4
1770 NEXT E1
1780 I3=S4*E2/3
1790 RETURN
2000 CLOSE
2005 END
```

VZ= .215 B= 2.61 C= 1.58 D+= 2.60000E-04

K	N(1/B)	N'(1/B)	N'(S)	G(S)	F1	F2	F3
0	.8	.316	1.36015	.963604	.0106003	4.47725E-21	1.98365E-07
0	.81	.3002	1.37446	.95822	.0103119	4.42379E-21	1.90486E-07
0	.82	.2844	1.38795	.952261	.0100234	4.36136E-21	1.82553E-07
0	.83	.2686	1.40057	.945685	9.73499E-03	4.29000E-21	1.74581E-07
0	.84	.2528	1.41223	.938453	9.44655E-03	4.20976E-21	1.66586E-07
0	.85	.237	1.42283	.930521	9.15811E-03	4.12073E-21	1.58583E-07
0	.86	.2212	1.43229	.921846	8.86966E-03	4.02305E-21	1.50588E-07
0	.87	.2054	1.44047	.912383	8.58122E-03	3.91690E-21	1.42619E-07
0	.88	.1896	1.49327	.896609	8.14855E-03	3.85375E-21	1.32681E-07
0	.89	.1738	1.49983	.88497	7.66011E-03	3.72878E-21	1.24815E-07
0	.9	.158	1.55545	.865704	7.42744E-03	3.64177E-21	1.15000E-07
0	.91	.1422	1.55998	.851579	7.13900E-03	3.49926E-21	1.07332E-07
0	.92	.1264	1.61873	.828338	6.70634E-03	3.38988E-21	9.77662E-08
0	.93	.1106	1.68145	.80247	6.27367E-03	3.26849E-21	8.83760E-08
0	.94	.0948	1.74869	.773782	5.84100E-03	3.13567E-21	7.92032E-08
0	.95	.079	1.82111	.742078	5.40834E-03	2.99209E-21	7.02900E-08
0	.96	.0632	1.89943	.707153	4.97567E-03	2.83849E-21	6.16787E-08
0	.97	.0474	2.07609	.655209	4.39878E-03	2.69951E-21	5.15097E-08
0	.98	.0316	2.17889	.611934	3.96612E-03	2.52534E-21	4.36949E-08
0	.99	.0158	2.41357	.548049	3.38923E-03	2.36085E-21	3.45583E-08

1	.8	.316	1.6911	.984562	.0121868	6.14670E-21	2.77099E-07
1	.81	.3002	1.65409	.983175	.0120425	5.96772E-21	2.68941E-07
1	.82	.2844	1.6553	.980124	.0117541	5.87877E-21	2.58859E-07
1	.83	.2686	1.64932	.976674	.0114557	5.75884E-21	2.48289E-07
1	.84	.2528	1.63523	.972794	.0111772	5.60616E-21	2.37237E-07
1	.85	.237	1.61183	.96845	.0108888	5.41849E-21	2.25693E-07
1	.86	.2212	1.57755	.963604	.0106003	5.19290E-21	2.13631E-07
1	.87	.2054	1.57305	.955315	.0101677	5.00358E-21	1.99050E-07
1	.88	.1896	1.50911	.949052	9.87922E-03	4.68283E-21	1.85772E-07
1	.89	.1738	1.50977	.934577	9.30233E-03	4.43700E-21	1.67782E-07
1	.9	.158	1.48183	.917215	8.72544E-03	4.09621E-21	1.48892E-07
1	.91	.1422	1.4554	.890906	8.00433E-03	3.68747E-21	1.26948E-07
1	.92	.1264	1.40124	.851579	7.13900E-03	3.14318E-21	1.01724E-07
1	.93	.1106	1.38269	.76356	5.69678E-03	2.41002E-21	6.73078E-08
1	.94	.0948	1.23767	.375707	2.09123E-03	7.58696E-22	1.04156E-08

SLN NOT POSSIBLE AT N= .95

2	.8	.316	2.03233	.992024	.0131963	7.71949E-21	3.43740E-07
2	.81	.3002	1.99986	.991173	.0130521	7.55463E-21	3.35291E-07
2	.82	.2844	2.01828	.989271	.0127637	7.53517E-21	3.25419E-07
2	.83	.2686	1.9684	.988212	.0126194	7.30294E-21	3.15752E-07
2	.84	.2528	1.96426	.985861	.012331	7.19062E-21	3.04222E-07
2	.85	.237	1.89263	.984562	.0121868	6.87919E-21	2.93145E-07
2	.86	.2212	1.86007	.981697	.0118983	6.65923E-21	2.79791E-07
2	.87	.2054	1.80908	.978451	.0116099	6.37158E-21	2.65318E-07
2	.88	.1896	1.78422	.972794	.0111772	6.11694E-21	2.47809E-07
2	.89	.1738	1.72855	.966092	.0107445	5.75111E-21	2.28660E-07
2	.9	.158	1.6327	.95822	.0103119	5.25497E-21	2.07611E-07
2	.91	.1422	1.56751	.942154	9.59077E-03	4.73753E-21	1.80083E-07
2	.92	.1264	1.44282	.917215	8.72544E-03	3.98836E-21	1.46919E-07
2	.93	.1106	1.2937	.851579	7.13900E-03	2.90195E-21	9.77426E-08

SLN NOT POSSIBLE AT N= .94

APPENDIX B

PROGRAM FOR ANALYZING RELAXATION CURRENT DATA FROM THE PULSE HEIGHT ANALYZER

The principle of the analysis was discussed in the experiment and will not be repeated here. The programming features included using an INPUT statement to input the information stored in the pulse height analyzer memory. The character file from the PHA was converted to a numeric file-- it is important that the format from a given PHA is identical to that of the Northern Econ II as otherwise it is unlikely the program will work. Modification of lines 42 to 85 could rectify this problem if it arose. The format of the information accumulated by the PHA should be as shown in Fig. A.1. Variations of the data structure could require further program changes. Least squares was used to fit the appropriate curves to sections of the data. Details of the fitted curves are given in section 3.4 and referred to in the REMark statements inserted in the program.

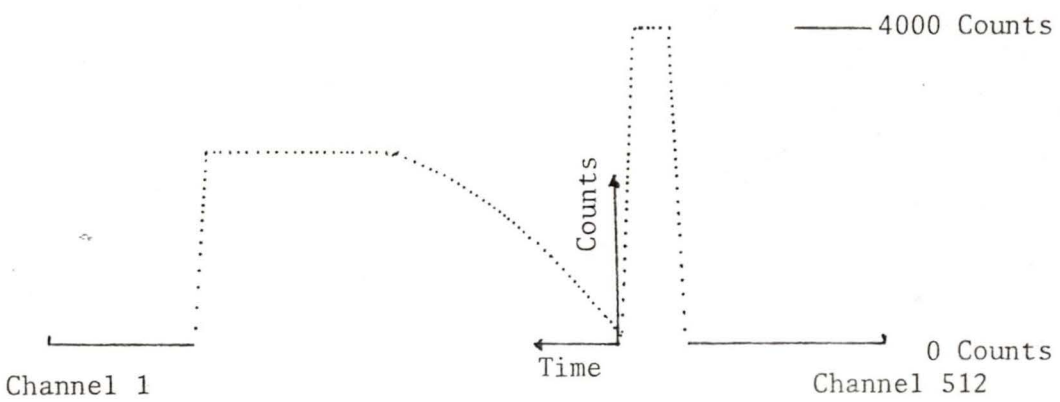

Figure A.1. A Typical Signal Accumulated in the PHA

```
5 REM-  PROGRAM TO DETERMINE RELAXATION TIME FROM DATA
6 REM-  ACCUMULATED ON NORTHERN PULSE HEIGHT ANALYSER.
10 REM -FIRST INPUTTING NEW DATA,REMOVE LINE 17
11 D=8 \ F=106 \ G=0
12 FOR D1=1 TO 2
13 REM-A.DC IS A CHARACTER FILE FROM PULSE HEIGHT ANALYSER
14 REM-ARRAY.DC IS A NUMERIC FILE CREATED FROM A.DC
15 OPEN 'DK0:A.DC' FOR INPUT AS FILE VF1$(256)=60
16 OPEN 'ARRAY.DC' FOR OUTPUT AS FILE VF2%(500)
17 GO TO 42
18 REM-  LINES 20 & 30 INPUT FROM PULSE HEIGHT ANALYSER
19 REM-  (ENSURE BAUD RATES OF PHA AND COMPUTER PORT ARE MATCHED)
20 FOR K=1 TO 205 \ INPUT J$ \ VF1(K)=J$ \ NEXT K \ CLOSE
30 GO TO 3500
35 REM-  LINES 42 TO 85 CREATE ARRAY.DC FROM A.DC
42 FOR I=0 TO 500 \ VF2(I)=0 \ NEXT I
50 FOR Q=D TO F \ P1=8 \ P2=11 \ E$=VF1(Q+1) \ W$=SEG$(E$,1,4) \ T=VAL(W$)
80 FOR N=0 TO 4 \ B=VF2(0) \ D$=SEG$(E$,P1,P2) \ VF2(B)=VAL(D$)
85 P1=P1+7 \ P2=P2+7 \ VF2(0)=VF2(0)+1 \ NEXT N
130 NEXT Q \ CLOSE  \ OPEN 'ARRAY.DC' FOR INPUT AS FILE VF2%(500)
134 REM-  LINE 140 SEARCHES FOR BEGINNING OF SIGNAL DATA
140 FOR T1=1 TO 300 \ IF (VF2(T1+1)-VF2(T1))>50 GO TO 150 \ NEXT T1
141 REM-
142 REM-  LINES 150 TO 260 LOCATE BEGINNING OF RELAXATION DATA
143 REM-
150 B1=T1+1
200 M1=1.00000E+10
210 FOR T1=(B1+100) TO 500
220 REM-
221 REM-  MAXIMUM ACCUMULATED SIGNAL ON PHA LIMITED TO 4000
222 REM-  COUNTS.  USE THIS FACT TO FIND SIGNAL EDGE.
223 REM-
230 IF VF2(T1)>3900 GO TO 280
240 IF VF2(T1)>M1 THEN 260
250 M1=VF2(T1) \ B3=T1
260 NEXT T1
270 REM-
272 REM-  LINE 280 IS COARSE LOG FIT TO RELAXATION SIGNAL
273 REM-
280 B2=B3-20 \ G2=10 \ S7=VF2(B2) \ G3=100 \ GOSUB 2000
281 REM-  LINES 282 TO 287 IS THE SECOND LOG FIT
282 G2=10 \ G3=84
284 P7=INT(A3/5)
286 S7=VF2(B2)+A4+A3*LOG(P7)
287 B2=B2-P7 \ GOSUB 2000
288 GOSUB 1000
294 PRINT ,'LINE EQN IS  Y=',A1,'X +',A2
300 PRINT ,'RELAX. REGION EQN IS  Y=',A4,'+',A3,'LN(X)'
350 GOSUB 3000
360 REM-
361 REM-  FIRST TERM OF T2 IS THE TIME WIDTH (MSEC.) OF THE
362 REM-  ACCUMULATED DATA (15 MSEC SHOWN)
363 REM-
420 T2=15*(B2-B2+Z)/(B3-B1)
```

```
425 CLOSE
430 PRINT 'CHANNEL',D1,'TIME=',T2 \ D=110 \ F=202 \ NEXT D1
450 GO TO 4000
500 REM-
501 REM-  LINES 1000 TO 1050 FIT STRAIGHT LINE TO EQUILIBRIUM DATA
502 REM-
1000 P0=0 \ P1=0 \ P2=0 \ P3=0 \ P4=0
1010 FOR C1=(B1+10) TO (B1+109)
1012 F9=VF2(C1)-S7
1015 P0=P0+B2-C1 \ P1=P1+F9 \ P2=P2+(B2-C1)↑2
1020 P4=P4+(B2-C1)*F9 \ NEXT C1
1030 A1=(100*P4-P0*P1)/(100*P2-P0↑2)
1040 A2=(P1*P2-P0*P4)/(100*P2-P0↑2)
1050 RETURN
1500 REM-
1501 REM- LINES 2000 TO 2080 FIT LOG CURVE TO RELAXATION DATA
1502 REM-
2000 P0=0 \ P1=0 \ P2=0 \ P3=0 \ P4=0
2010 FOR C1=G2 TO G3
2015 F1=VF2(B2-C1)-S7
2020 P0=P0+LOG(C1) \ P4=P4+LOG(C1)*F1
2030 P1=P1+F1 \ P2=P2+(LOG(C1))↑2 \ NEXT C1
2040 Q9=G3-G2+1
2050 A3=(Q9*P4-P0*P1)/(Q9*P2-P0↑2)
2060 A4=(P1*P2-P0*P4)/(Q9*P2-P0↑2)
2080 RETURN
2500 REM-
2501 REM-  LINES 3000 TO 3030 USE THE NEWTON RAPHSON METHOD
2502 REM-  TO CALCULATE THE TIME OF INTERSECTION OF THE
2503 REM-  STRAIGHT LINE FITTED TO THE EQUILIBRIUM DATA AND
2504 REM-  THE LOG CURVE FITTED TO THE RELAXATION DATA.
3000 DEF FNA(Z)=A4-A2+A3*LOG(Z)-A1*Z
3010 DEF FNB(Z)=A3/Z-A1
3015 Z=A3/A1
3016 IF FNA(Z)<0 THEN 3040
3017 Z=80
3020 IF ABS(FNA(Z))<.1 THEN 3050
3030 Z=Z-FNA(Z)/FNB(Z) \ GO TO 3020
3035 GO TO 3050
3040 PRINT "NO INTERSECTION"
3050 RETURN
3500 PRINT 'PUT IN LINE 17 AS GO TO 42, AND RUNNH'
4000 CLOSE  \ END
```

VITA

Surname: GILES Given Names: CLINTON RANDY

Place of Birth: VANCOUVER, B.C. Date of Birth: MAY 8, 1955

Educational Institutions Attended, with Dates of Entering and Leaving:

Univ. of Victoria, Victoria, B.C.	1972 to	1976
Univ. of Victoria, Victoria, B.C.	1976 to	present
	to	
	to	

Degrees, Diplomas, Etc., Awarded, with Dates and Names of Institutions:

B.Sc.	1976	Univ. of Victoria, B.C.

Honors and Awards:

National Research Council Scholarship 1976/77 and 1977/78

Publications:

PARTIAL COPYRIGHT LICENSE

I hereby grant the right to lend my thesis or dissertation (the title of which is shown below) to users of the University of Victoria Library, and to make *single copies only* for such users or in response to a request from the library of any other university, or similar institution, on its behalf or for one of its users. I further agree that permission for extensive copying of this thesis for scholarly purposes may be granted by me or a member of the University designated by me. It is understood that copying or publication of this thesis for financial gain shall not be allowed without my written permission

Title of Thesis/Dissertation

Flush Probe Studies of Plasma Flow Aver A Flat Plate

Author [redacted]

Signature

Clinton Randy Giles

Name

August 17, 1978

Date